

Technical Report No. 4

SPECIAL STUDIES OF AROD SYSTEM
CONCEPTS AND DESIGN

GPO PRICE \$ _____

CFSTI PRICE(S) \$ _____

Contract NAS8-20128

Hard copy (HC) 3.00Microfiche (MF) 65

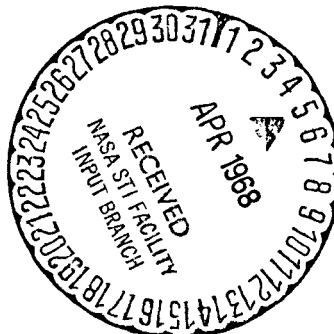
July 31, 1967

ff 653 July 65

Prepared for

National Aeronautics and Space Administration
George C. Marshall Space Flight Center
Huntsville, Alabama 35812**ADVANCED COMMUNICATIONS
INFORMATION MANAGEMENT**

N68-19632
(ACCESSION NUMBER)
72
(PAGES)
NASA-CR-61670
(NASA CR OR TMX OR AD NUMBER)
07
(CODE)
(CATEGORY)
FACILITY FORM 602

**RESEARCH
DEVELOPMENT
ENGINEERING**

ADCOM, INC.

WESTERN DIVISION
PALO ALTO, CALIFORNIA
(415) 328-0200808 MEMORIAL DRIVE
CAMBRIDGE, MASSACHUSETTS 02139
(617) 868-1000WASHINGTON BRANCH
COLLEGE PARK, MARYLAND
(301) 779-4666

50T 50492

Technical Report No. 4

SPECIAL STUDIES OF AROD SYSTEM
CONCEPTS AND DESIGNS

Contract NAS 8-20128

July 31, 1967

Prepared for

National Aeronautics and Space Administration
George C. Marshall Space Flight Center
Huntsville, Alabama 35812

Authors

D. Bradley Crow
Ahmad F. Ghais
S. Ahmed Meer

Approved by Steven M. Sussman
Steven M. Sussman
Director of Research

Submitted by

ADCOM, Inc.
808 Memorial Drive
Cambridge, Massachusetts 02139

PRECEDING PAGE BLANK NOT FILMED.

TABLE OF CONTENTS

Section		Page
1	INTRODUCTION SUMMARY	1
2	AROD RANGE-CODE PROPERTIES.	3
	2.1 Introduction	3
	2.2 Properties of P-N Sequences	5
	2.3 Combined Code Correlation Function.	7
	2.4 Correlation Function of $L^{\oplus} F_L$	13
3	VTR ACQUISITION ANALYSIS	18
	3.1 Introduction	18
	3.2 Acquisition State V-1	21
	3.3 Acquisition State V-3	28
4	ATMOSPHERIC PROPAGATION EFFECTS ON AROD RANGING ERRORS	30
	4.1 Introduction	30
	4.2 The Propagation Effects	30
	4.3 Review of Some Previous Findings	31
	4.4 Ranging Errors From Tropospheric Propagation.	33
5	POSITION DETERMINATION WITH THE AROD SYSTEM.	38
	5.1 Introduction	38
	5.2 Geodetic Considerations	39
	5.2.1 Reference Surfaces	39
	5.2.2 Geodetic Surveys	42
	5.2.3 Application to Space Tracking Operations.	45
	5.3 In-Flight Computer Coordinate System	47
	5.4 Station Coordinate Translation.	47
	5.5 Vehicle Position Computation	55
	5.6 Vehicle Position Errors Due to Inaccuracies in Station Coordinates	61
	5.6.1 Local Control Errors	62
	5.6.2 Errors to Datum Origin.	62
	5.6.3 Errors to Earth's Center	62
	5.6.4 Positional Accuracy of Ground Stations	63
	5.6.5 Conclusions.	63

TABLE OF CONTENTS (Cont.)

Section		Page
5.7	Recommendations for Further Study.	64
	REFERENCES.	66

LIST OF ILLUSTRATIONS

Figure		Page
1	Combined AROD Ranging-Code	4
2	Correlation Functions and Power Spectrum of L and H Codes (Not to scale)	6
3	Properties of H	8
4	$A(t, \tau) = C(t) C(t + \tau)$	10
5	Correlation Function of Combined Code	11
6	Envelopes of Main Components of $\Phi_{CC}(f)$	11
7	Autocorrelation Function $\phi_{CC}(\tau)$ Computed by Motorola	14
8	Computation of Correlation of $L \oplus F_L$	15
9	Correlation Function of $L \oplus F_L$	16
10	Spectra for $L \oplus F_L$	17
11	VTR Carrier and Range Code Loop	19
12	Effect of Carrier Loop Bandwidth on Correlation Function of L Code (From Ref. 2, Fig. 15).	26
13	Refractive Propagation through the Troposphere	34
14	Meridional Section (From Ref. 9).	40
15	Vectors Involved in Position Determination of Space Vehicles	46
16	Computer Coordinate System	48
17	Geometry of Ground Station Coordinate Translation	50
18	Transformation of Station Coordinate to Earth-Center, Rectangular Coordinate System	51
19	Rotation of Coordinate System About Z''' Axis	53
20	Rotation of Coordinate System About X_a'' Axis	53

1. INTRODUCTION AND SUMMARY

This report constitutes the Fourth Technical Report on the results of a program of investigations carried out by ADCOM, Inc. under Contract No. NAS8-20128 for George C. Marshall Space Flight Center, Huntsville, Alabama. The work covered in this report was conducted in close coordination with, and in direction support of, the Astrionics Division, George C. Marshall Space Flight Center.

The overall objective of the program is to investigate signaling and signal processing techniques for the AROD system that will most simply and effectively yield unambiguous range and range-rate measurements, within the limitations of existing sources of error, and in harmony with other vehicle and ground station instrumentation functions. The result of the investigations will aid NASA in the planning, design, and implementation of the AROD tracking system.

The specific subjects of this report are three:

- a) Evaluation of the signal acquisition procedure employed in the AROD Vehicle Tracking Receiver (VTR).
- b) Evaluation of the ranging errors incurred by propagation through the atmosphere, and of the possibility of correcting them in subsequent data processing.
- c) Consideration of some geodetic aspects relating to position determination with the AROD system, including ground station coordinate system translation and fixing computations required of a vehicle-borne computer.

In Section 2 some correlation properties of the AROD ranging code are derived. These properties are central to the discussion of VTR signal acquisition, which is presented in Section 3. Here, the emphasis is to explain test results obtained by Motorola, Inc., and to suggest techniques for improving critical phases of the acquisition procedure.

The range errors incurred by propagation through the atmosphere are evaluated in Section 4. Both tropospheric and ionospheric error sources are considered. Only simple and approximate bounds to these errors are derived, in order to indicate the magnitude of the problem. The possibility and merits of gross range corrections are then explored.

The AROD vehicle-borne system will include a computer which transforms the tracking measurements into parameters representing the vehicle velocity and position in space, utilizing geodetic information about the location of the transponders. This computation function is considered in detail in Section 5. First, geodetic terminology and the basics and meaning of geodetic measurements as related to AROD system fixing are discussed. Next, the mathematics for translation of ground station coordinates to the vehicle-borne computer coordinate system is treated. Finally, the mathematical process of vehicle position determination from station coordinates and AROD system measurements are covered, with a qualitative discussion of expected errors.

2. AROD RANGE-CODE PROPERTIES

2.1 Introduction

In this section we will derive properties of the AROD ranging code which are necessary for studying the VTR acquisition procedure. The second purpose of this section is to document in some detail the derivation of these properties in order to appreciate whether suggestions for modifications of the AROD code can be considered. The derivations of this section will be employed in Sec. 3.

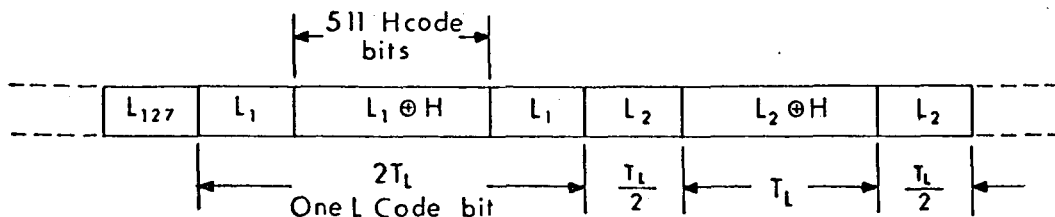
The following are the parameters of the code:

C-1. Clock frequency $f_H = 6.4 \text{ MHz}$

C-2. L Code 127 bit - PN sequence
 Bit Period $\Delta 2 T_L = \frac{1022}{f_H}$

C-3. H Code 511 bit - PN sequence
 Bit Period $\Delta T_H = \frac{1}{f_H}$

C-4. Form of Combined Code $C(t)$ (See Fig. 1)



R-3711



Fig. 1 Combined AROD Ranging-Code

C-5. Period of Code

$$T_r = 127 (2T_L) = 20 \text{ ms}$$

C-6. Maximum Range

$$R_m = \frac{1}{2} c T_r$$

$$= \frac{3 \times 10^8 \times 0.02}{2} = 3 \times 10^6 \text{ m}$$

2.2 Properties of P-N Sequences

The individual H and L codes are psuedo-noise sequences obtained from a linear shift register. For an n^{th} order shift register the maximum period is 2^{n-1} . The H and L codes have this maximum length, i. e., both codes are "maximum-length shift register sequences." These sequences satisfy three randomness properties.*

- P-1 (The Balance Property) In each period of the sequence the number of ONE's differs from the number of ZERO's by at most 1.
- P-2 (The Run Property) Among the runs of ONE's and of ZERO's in each period, one half the runs of each kind are of length one, one fourth of each kind are of length two, one eighth are of length three and so on as long as the fractions give meaningful number of runs.
- P-3 (The Correlation Property) If a period of the sequence is compared term by term with any cyclic shift of itself, the number of agreements differs from the number of disagreements by at most 1.

The correlation function of the individual H and L codes using the above properties can be shown to be a series of triangular pulses as shown in Fig. 2. There is a small negative dc component in the correlation function equal to $1/(\text{period in bits})^2$ and hence is negligibly small. The corresponding power density spectra for the two codes are

* Golomb, S.W., et. al., Digital Communications with Space Applications, Prentice Hall, Inc., New York, 1964.

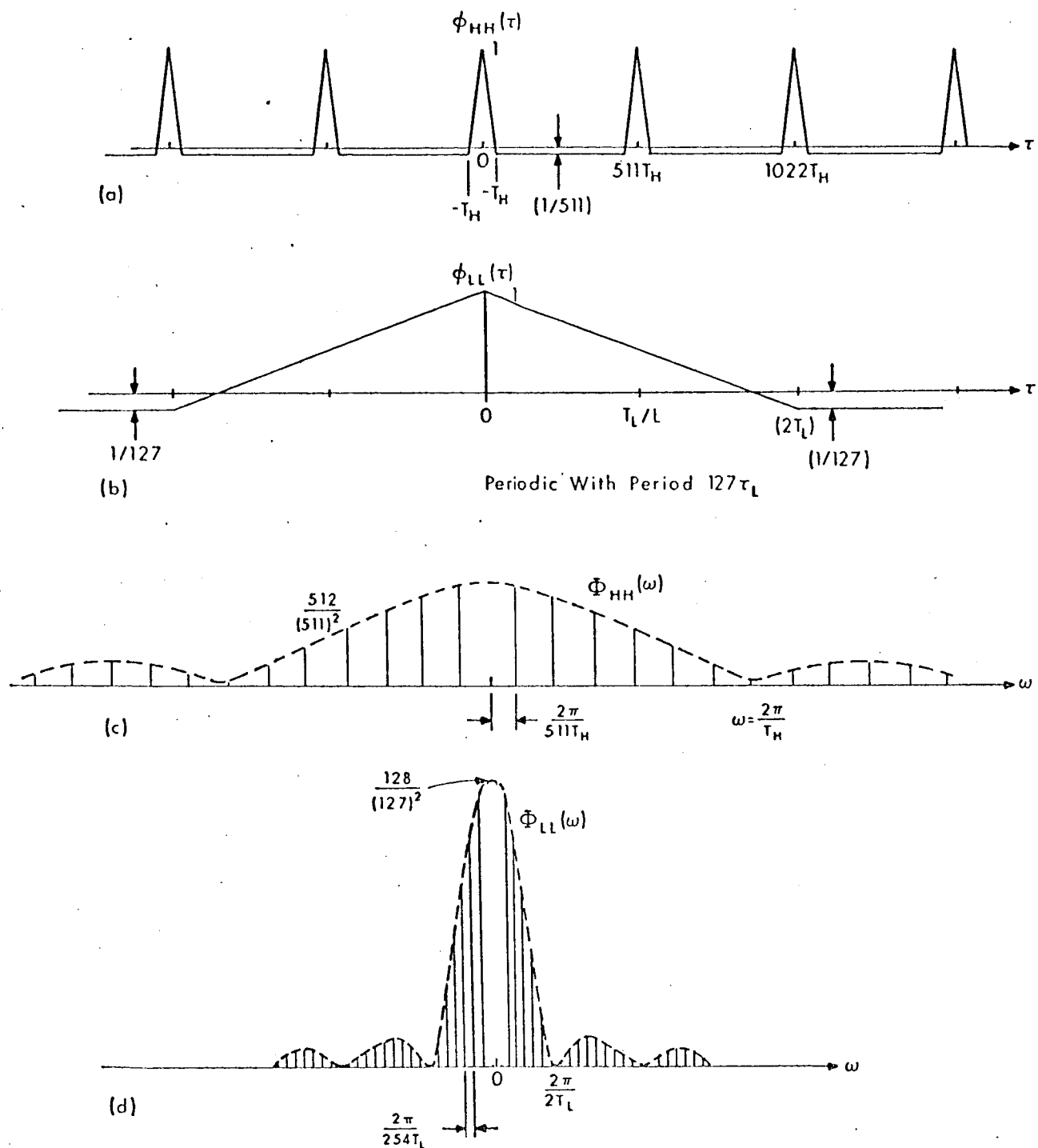


Fig. 2. Correlation Functions and Power Spectrum of L and H Codes (Not to scale)

$$\Phi_{HH}(\omega) = \frac{512}{(511)^2} \left[\frac{\sin(\omega T_H/2)}{\omega T_H/2} \right]^2 \sum_{\substack{n=-\infty \\ n \neq 0}}^{+\infty} \delta\left(\omega - \frac{2\pi n}{511 T_H}\right) + \frac{\delta(\omega)}{(511)^2} \quad (1)$$

$$\Phi_{LL}(\omega) = \frac{128}{(127)^2} \left[\frac{\sin(\omega T_L)}{\omega T_L/2} \right]^2 \sum_{\substack{n=-\infty \\ n \neq 0}}^{+\infty} \delta\left(\omega - \frac{2\pi n}{254 T_L}\right) + \frac{\delta(\omega)}{(127)^2} \quad (2)$$

(Note: L code period $\triangleq 2 T_L$)

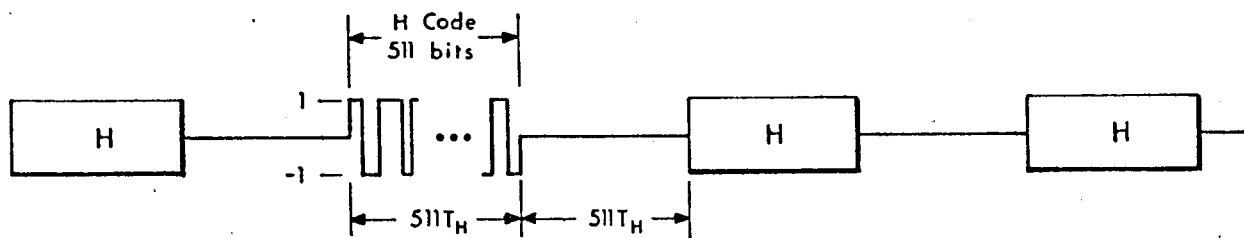
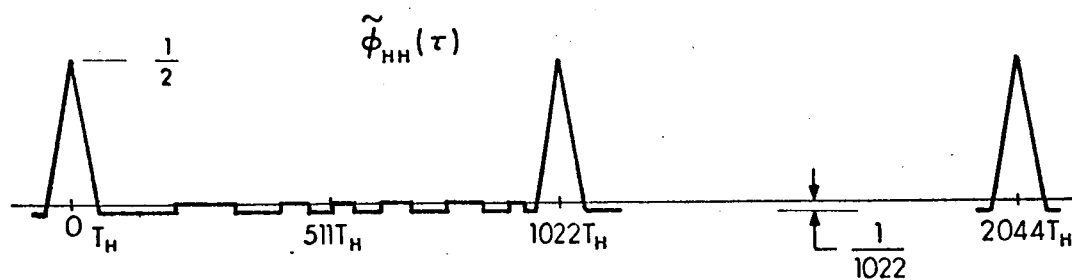
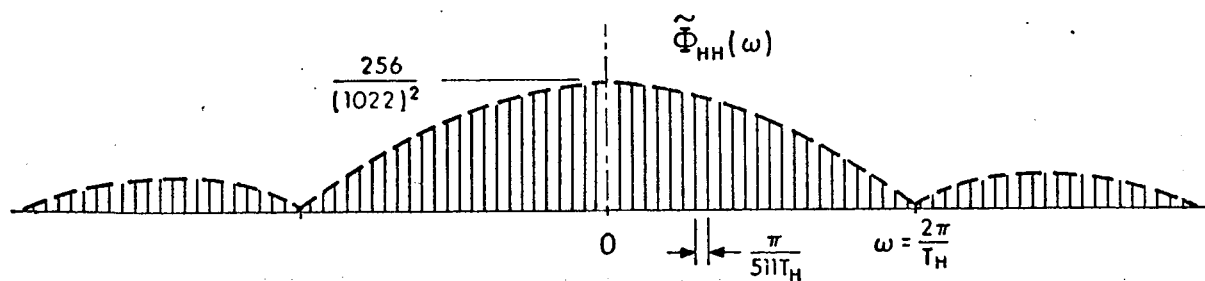
where $\delta(\omega)$ is the unit impulse. The spectral density for each component is also plotted in Fig. 2.

2.3 Combined Code Correlation Function

Before computing the correlation function and spectrum of the combined code, consider the waveform of Fig. 3a. The waveform is simply an amplitude modulated H code and we will denote it as \tilde{H} . Its correlation function $\tilde{\phi}_{HH}(\tau)$ can be sketched approximately as shown in Fig. 3b. There are a few differences from the correlation function of the H code $\phi_{HH}(\tau)$ which should be observed. First $\tilde{\phi}_{HH}(0)$ is half $\phi_{HH}(0)$ and the period of $\tilde{\phi}_{HH}(\tau)$ is double that of $\phi_{HH}(\tau)$. Furthermore, for shifts greater than $\pm T_H$, $\tilde{\phi}_{HH}(\tau)$ is not constant, as it is for $\phi_{HH}(\tau)$. Now it fluctuates between the values $1/1022$ and zero (using property P-3). Note that Fig. 3b shows only an approximate result.

The spectral density $\tilde{\Phi}_{HH}(\omega)$ is given by Fig. 3c.

$$\tilde{\Phi}_{HH}(\omega) = \frac{256}{(1022)^2} \left[\frac{\sin(\omega T_H/2)}{\omega T_H/2} \right]^2 \sum_{\substack{n=-\infty \\ n \neq 0}}^{+\infty} \delta\left(\omega - \frac{2\pi n}{1022 T_H}\right) + \frac{\delta(\omega)}{(1022)^2} \quad (3)$$

(a) Waveform \tilde{H} (b) Correlation Function of \tilde{H} (c) Spectral Density of \tilde{H}

R-3715

Fig. 3 Properties of \tilde{H}

The difference from that of $\Phi_{HH}(\omega)$ is that the separation between spectral lines is halved and the dc power is reduced by 1/4. However, because of equal bit period the envelope is still the same so that the first null of the envelope $\tilde{\Phi}_{HH}(\omega)$ is also at 6.4 MHz.

Let us now determine the correlation of the combined code $C(t)$ of Fig. 1. In order to compute this function we will first look at the product $A(t, \tau)$.

$$A(t, \tau) \triangleq C(t) C(t + \tau)$$

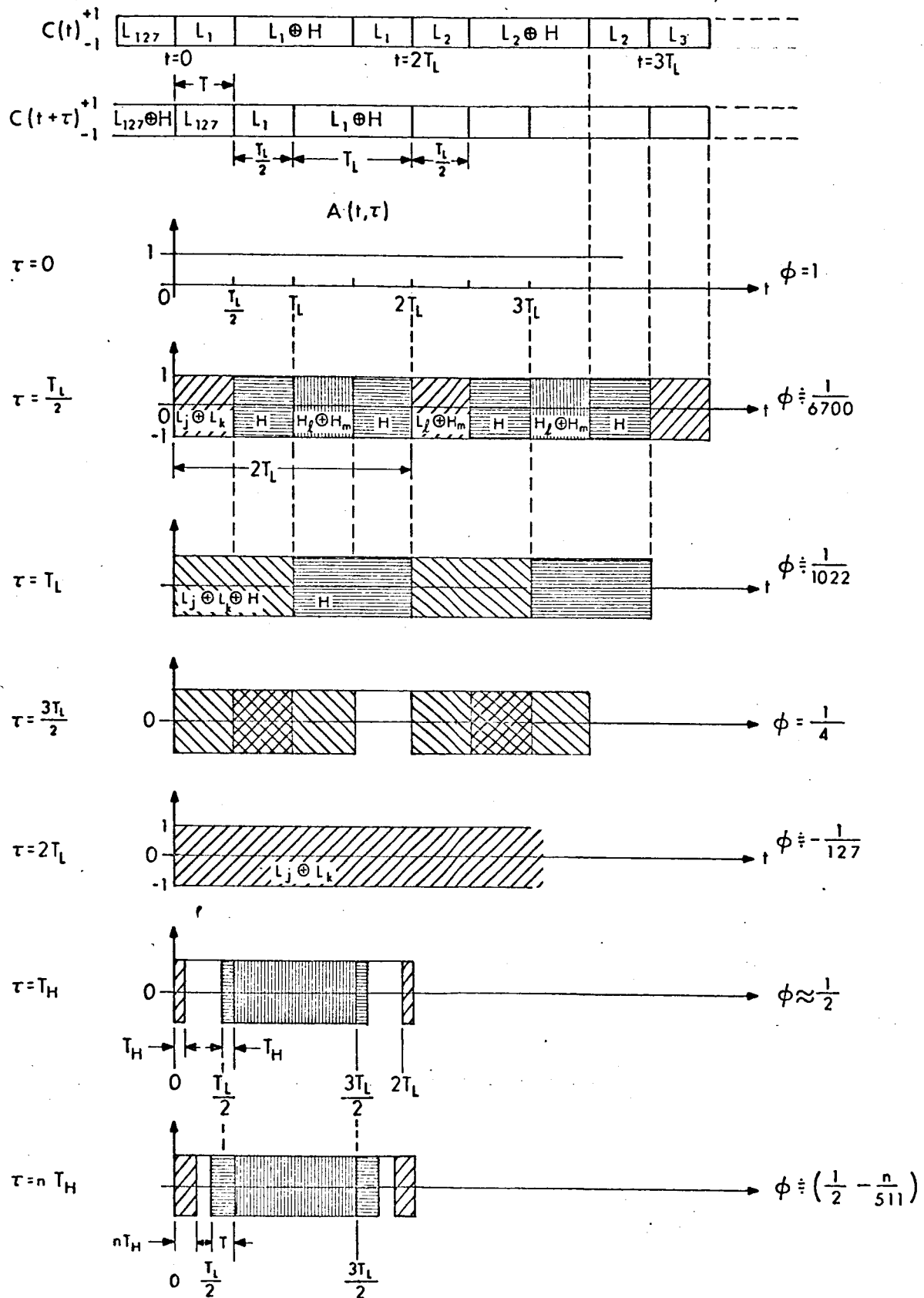
for different values of τ . Associated with $C(t)$ is a Boolean function C_t , such that when $C_t = 0$, $C(t) = +1$, and when $C_t = 1$, $C(t) = -1$. Thus the product $A(t, \tau)$ is correspondingly written in Boolean terms as $C_t \oplus C_{t+\tau}$ where \oplus denotes modulo 2 addition.

Since $C(t)$ is composed of PN sequences and we are only interested in the time average of $A(t, \tau)$,

$$\phi_{cc}(\tau) = \langle A(t, \tau) \rangle = \int_{\text{period}} A(t, \tau) d\tau \quad (4)$$

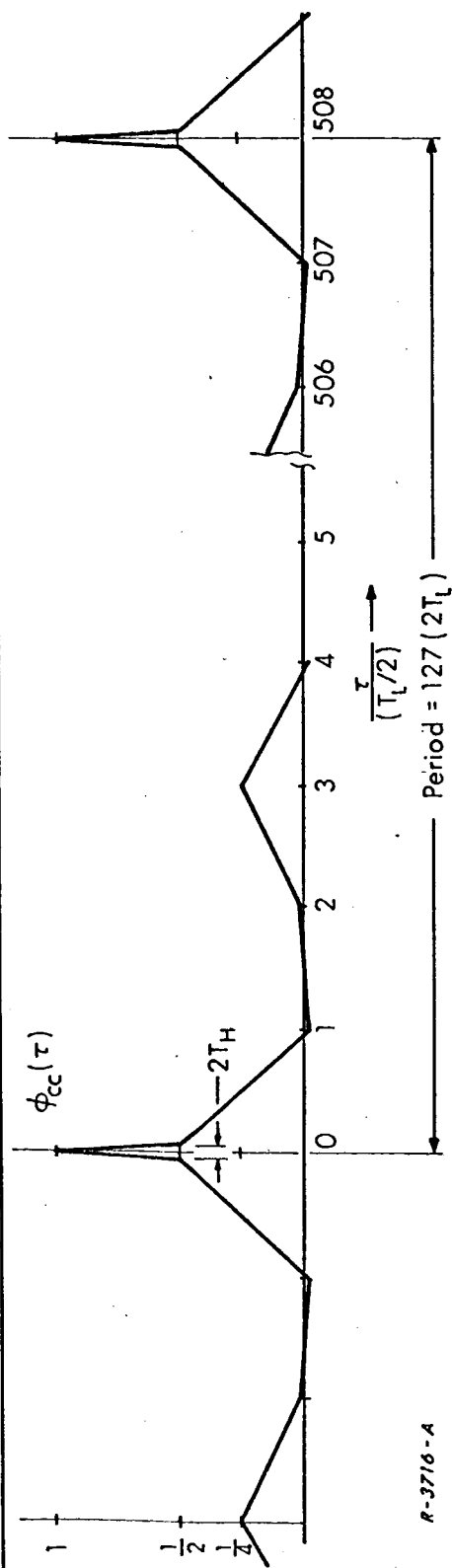
The computation of the correlation function involves only considering the following six possible categories in the table below. Once again it should be noted that the averages $\langle A(t, \tau) \rangle$ are approximate, the actual correlation function would have to be determined by direct computation.

In Fig. 4 $A(t, \tau)$ is plotted for various values of τ in terms of these categories, denoted by the different shadings of the table below. It will be observed that the shading pattern repeats every $2T_L$ sec; thus we need consider only one period of the L code to determine the average of $A(t, \tau)$. The resulting correlation function for the various values in Fig. 4 is plotted in Fig. 5. As an example of the computation consider the value of $\tau = nT_H$, where n is an integer between 1 and 255.



R-3714

Fig. 4 $A(t, \tau) = C(t)C(t + \tau)$



R-3716-A

Fig. 5 Correlation Function of Combined Code

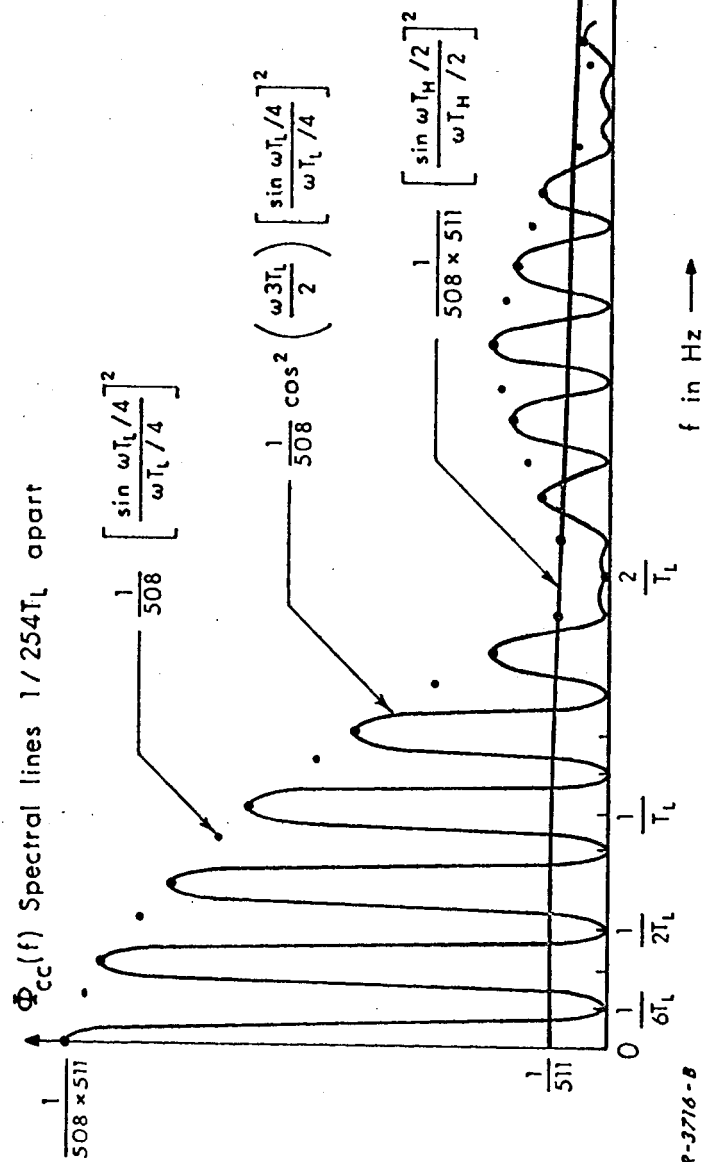
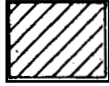
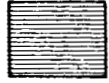
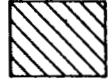




Fig. 6 Envelopes of Main Components of $\Phi_{CC}(f)$

No.	$A(t, \tau)$	$\langle A(t, \tau) \rangle$	Shading on Fig. 4
1	1	1	—
2	$L_j \oplus L_k$ $j \neq k$	$-\frac{1}{127}$	
3	$L_j \oplus L_j \oplus H = H$	$\frac{1}{511}$	
4	$L_j \oplus L_k \oplus H$ $j \neq k$	$-\frac{1}{(511)} \cdot \frac{1}{(127)}$	
5	$H_\ell \oplus H_m$ $\ell \neq m$	$-\frac{1}{511}$	
6	$L_j \oplus L_k \oplus H_\ell \oplus H_m$ $j \neq k, \ell \neq m$	$\frac{1}{(127)} \cdot \frac{1}{(511)}$	

$$\begin{aligned}
 \phi_{cc}(nT_H) &= \frac{1}{2T_L} \left\{ \frac{nT_H}{(127)} + (T_L - 2nT_H) + \frac{2nT_H}{(511)} \right\} \\
 &= \frac{1}{2} - n \left(1 - \frac{1}{511} - \frac{1}{254} \right) \frac{T_H}{T_L} \\
 &\approx \left(\frac{1}{2} - \frac{nT_H}{T_L} \right) = \frac{1}{2} - \frac{n}{511}
 \end{aligned} \tag{5}$$

Thus at $n = 255$, $\tau = T_L/2 - T_H \approx T_L/2$ and $\phi = 1/511$.

The spectral density of $\phi_{cc}(\tau)$ can be easily determined if the small variations of $\phi_{cc}(\tau)$ are neglected. Thus the approximate spectral density $\Phi_{cc}(\omega)$ of $\phi_{cc}(\tau)$ is (shown in Fig. 6)

$$\begin{aligned}
\Phi_{CC}(\omega) &= \frac{1}{2} \left\{ \frac{1}{(254)(511)} \left[\frac{\sin \omega T_H/2}{\omega T_H/2} \right]^2 + \frac{1}{2(254)} \left(1 + \cos \frac{\omega 3T_L}{2} \right) \left[\frac{\sin \omega T_L/4}{\omega T_L/4} \right]^2 \right\} \cdot \sum_{\substack{n=-\infty \\ n \neq 0}}^{+\infty} \delta \left(\omega - \frac{2\pi n}{254 T_L} \right) \\
&= \frac{1}{508} \left\{ \frac{1}{511} \left[\frac{\sin \omega T_H/2}{\omega T_H/2} \right]^2 + \cos^2 \frac{\omega 3T_L}{2} \left[\frac{\sin \omega T_L/4}{\omega T_L/4} \right]^2 \right\} \cdot \sum_{\substack{n=-\infty \\ n \neq 0}}^{+\infty} \delta \left(\omega - \frac{2\pi n}{254 T_L} \right) \quad (6)
\end{aligned}$$

It should be noted that $\phi_{cc}(\tau)$ derived here differs from that presented in "AROD System Description" by Motorola.¹ However, their digitally computed correlation function agrees with our $\phi_{cc}(\tau)$ as shown in Fig. 7.

2.4 Correlation Function of $L \oplus F_L$

In this section we derive the correlation function of the receiver generated code $L \oplus F_L$. This is the receiver-coder output in the acquisition state V-1. The correlation and spectral density of this waveform is useful in understanding the effects of carrier loop filtering during the above state. Let us denote this code waveform by $m_o(t)$ then the product function is

$$A_m(t, \tau) = m_o(t) m_o(t + \tau) \quad (7)$$

and the time average of this function gives the code autocorrelation function. In Fig. 2.8 $A_m(t, \tau)$ is plotted for different values of τ and corresponding values of $\phi_{mm}(\tau)$ are also given. The resulting correlation function is sketched in Fig. 2.9a. This function may be looked at approximately as the product of the two components shown in Fig. 2.9b, i. e., a periodic triangular wave $y(\tau)$ times the autocorrelation function of the L code $\phi_{LL}(\tau)$.

$$\phi_{mm}(\tau) \approx \phi_{LL}(\tau) \cdot y(\tau) \quad (8)$$

the spectrum of the triangular wave is impulses at odd harmonics of f_L shown in Fig. 10a. The corresponding spectral density¹ is then sketched in Fig. 10b.

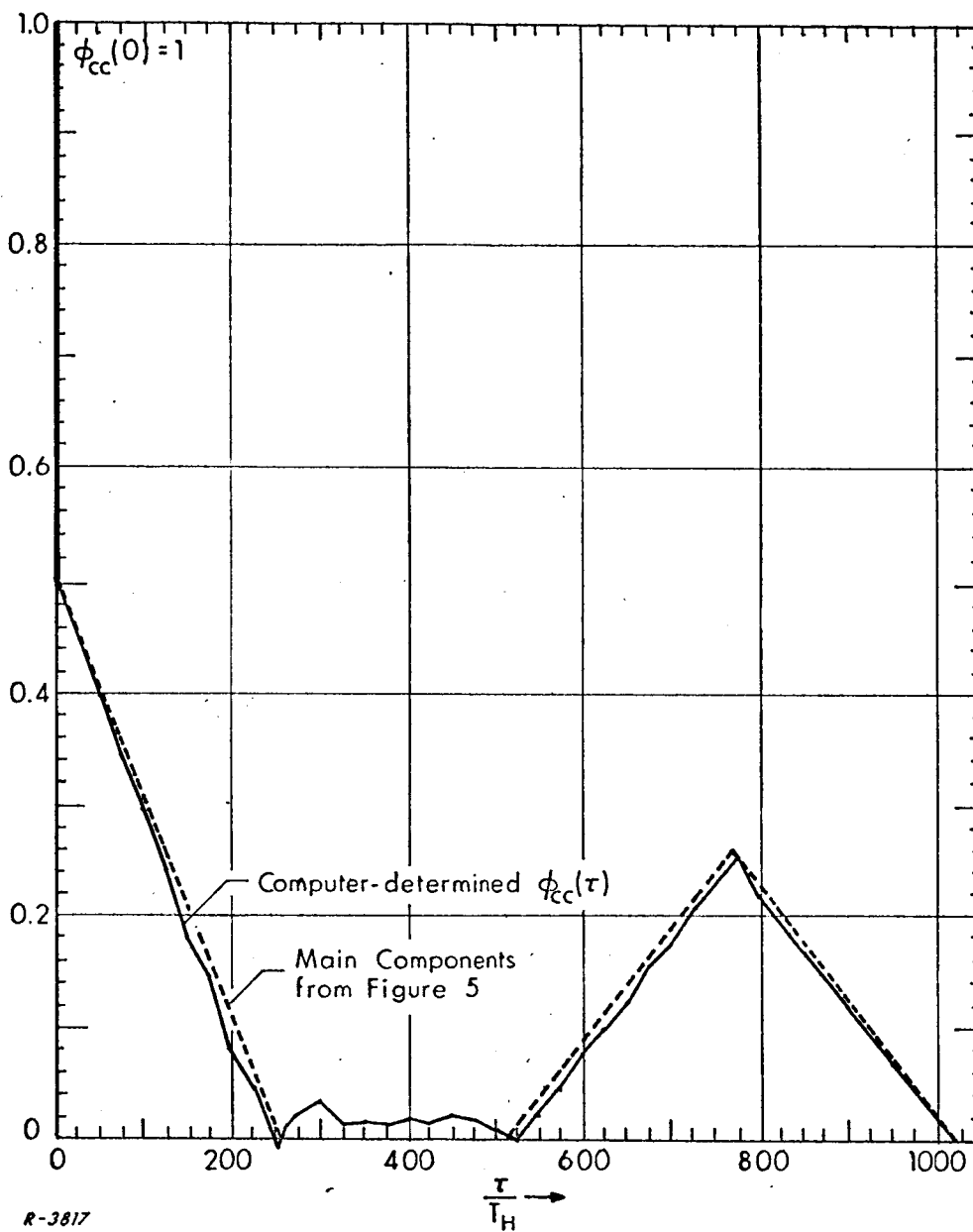
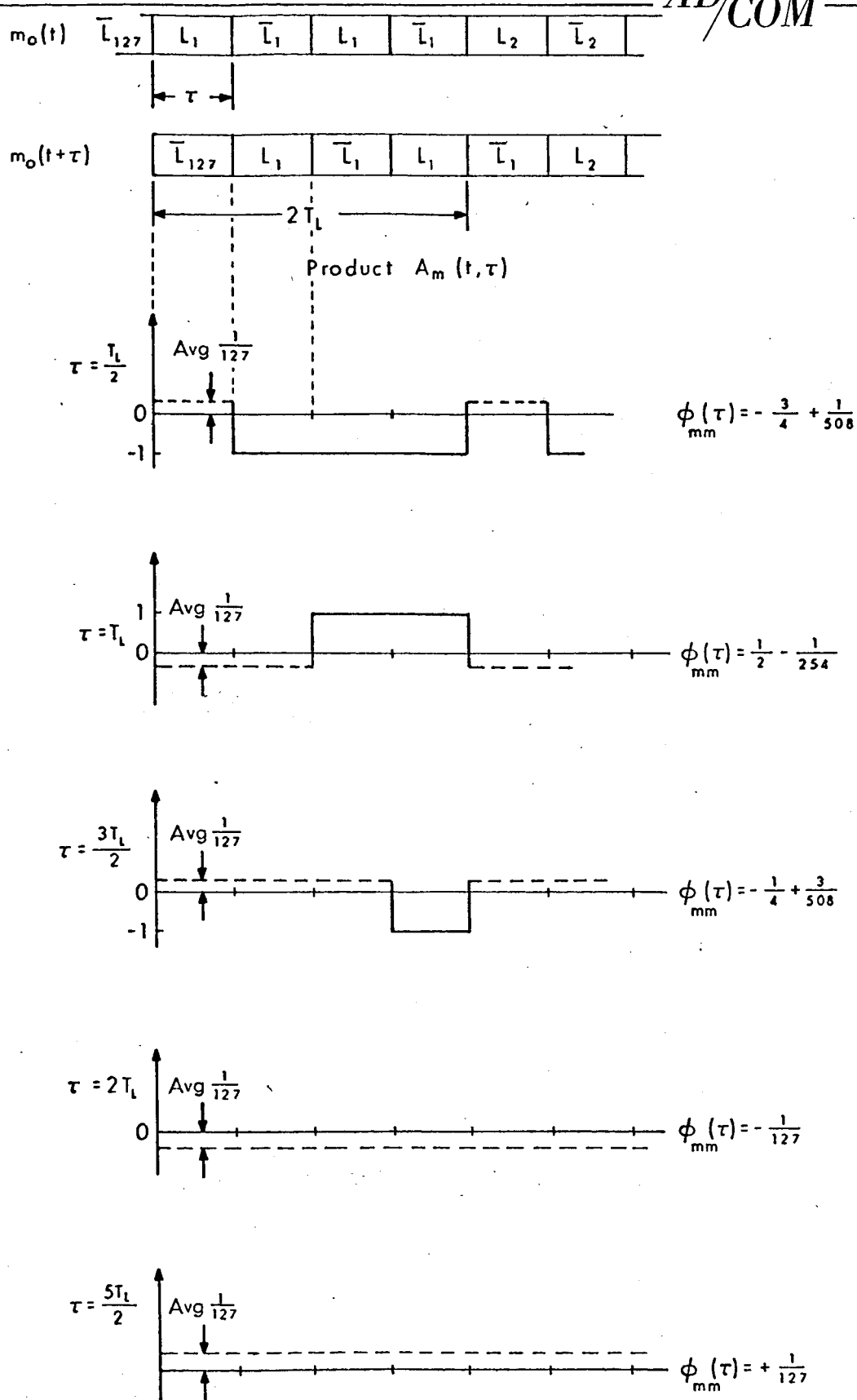
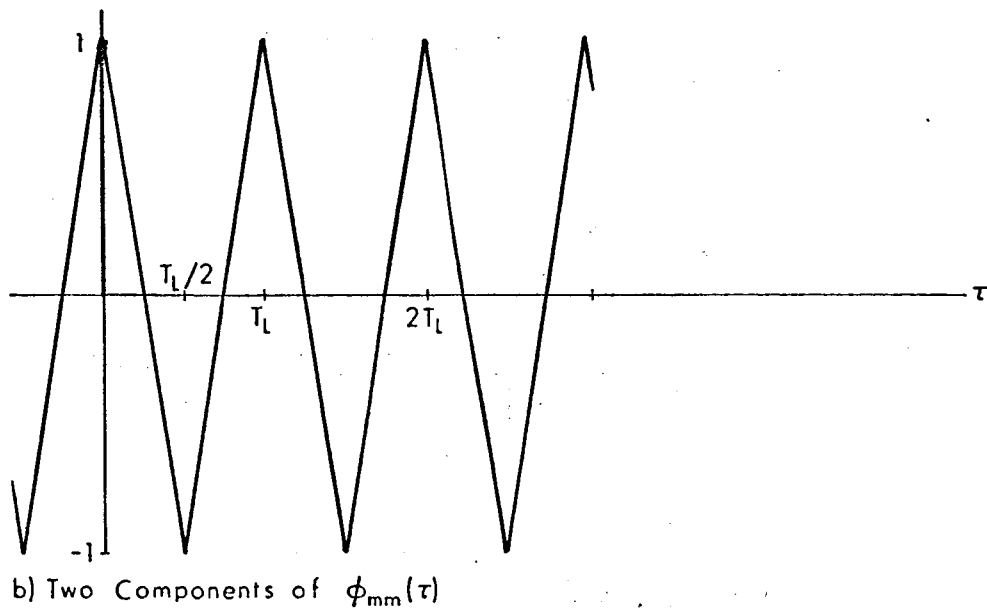
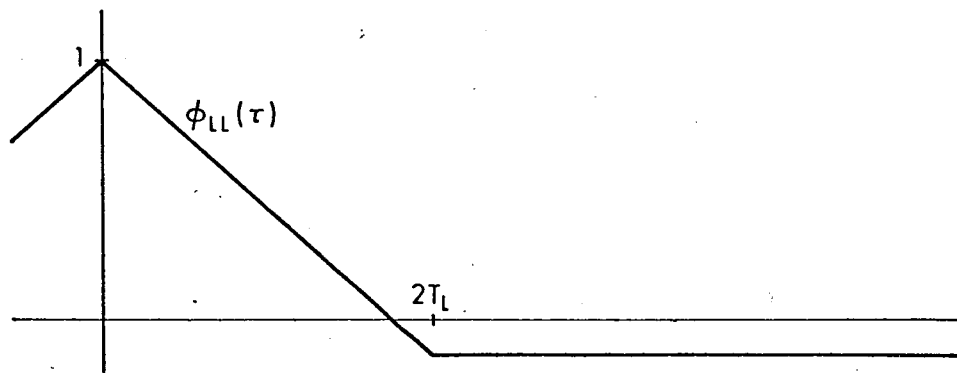
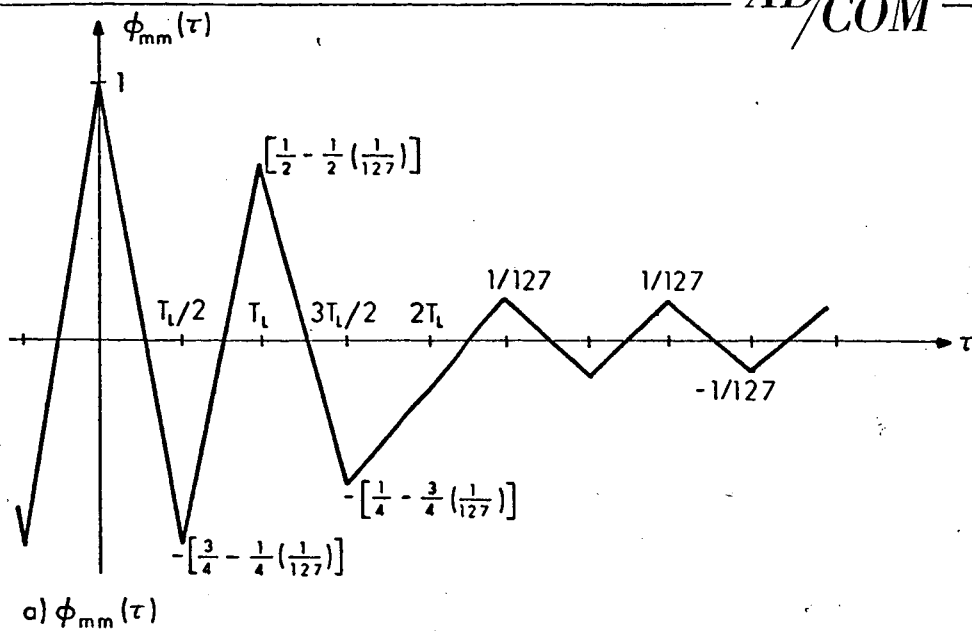


Fig. 7 Autocorrelation Function $\phi_{CC}(\tau)$ Computed by Motorola



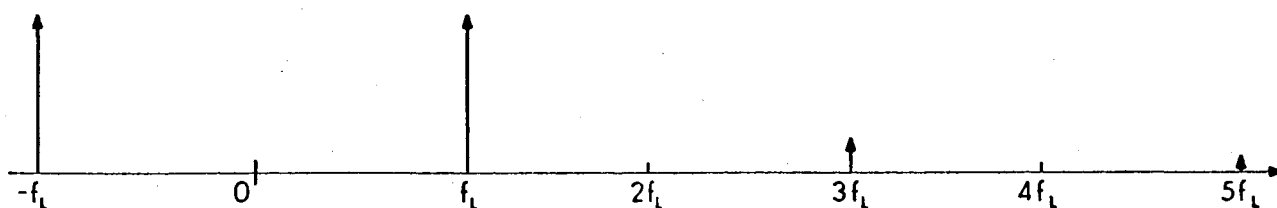
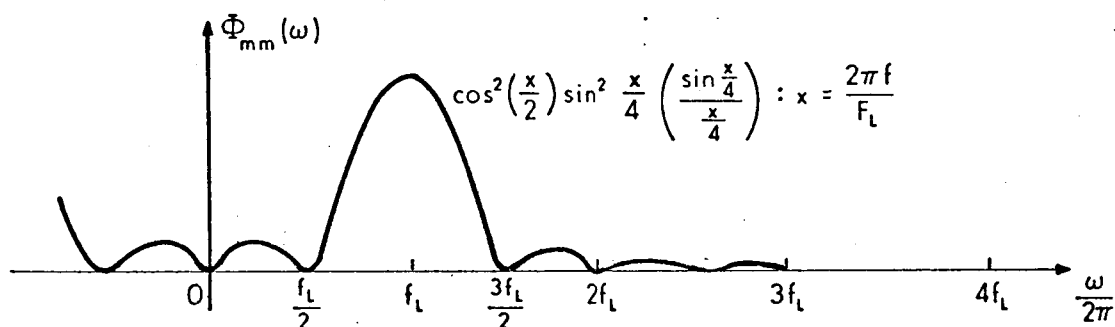
R-3766

Fig. 8 Computation of Correlation of $L \oplus F_L$



R-3767

Fig. 9 Correlation Function of $L \oplus F_L$

a) Spectrum of $y(\tau)$ b) Spectral Density of $L \oplus F_L$

R-3768

Fig. 10. Spectra for $L \oplus F_L$

The need for determining the spectrum of this code and those of the earlier sections will be appreciated when we analyze the VTR acquisition procedure in the next section.

3. VTR ACQUISITION ANALYSIS

3.1 Introduction

In this section we analyze the acquisition process in the Vehicle Tracking Receiver (VTR). The object of the analysis is to explain test results obtained by Motorola, Inc. and to suggest techniques for improving critical phases of the acquisition procedure.

The essential configuration^{1,2} of the VTR is drawn in Fig. 11. It consists of two loops, a range loop and a carrier loop. This arrangement performs both carrier and code tracking once synchronization has been achieved. Code synchronization is done by shifting the code to the position that indicates maximum correlation, while the carrier loop acquires with the use of a discriminator aid. Initially the carrier doppler of the received signal is small, being about ± 500 Hz. This is considerably lower than the actual two-way-doppler due to the doppler reverse technique. In Fig. 11 we have shown dotted various gates that are employed in the system. The necessity of the gates arises because the system is time-shared for L code and H code tracking.

The input signal of the VTR is a carrier phase-modulated by a binary waveform $m_1(t) = \pm 1$. This modulation being bi-level $\pm 90^\circ$, we can write the input signal as

$$\begin{aligned} e_s(t) &= \cos\left(\omega_1 t + \theta_1(t) + \frac{\pi}{2} m_1(t)\right) \\ &= m_1(t) \sin\left(\omega_1 t + \theta_1(t)\right) \end{aligned} \quad (9)$$

Thus, the input signal may be viewed also as an amplitude modulated carrier. The zero doppler input frequency is $(\omega_1/2\pi)$ Hz and $\theta_1(t)$ is a time varying phase due to doppler. $m_1(t)$ is the range code which has two different forms depending on the acquisition stage. This input signal is multiplied by the receiver generated code $m_0(t)$ which also has different forms in the different acquisition stages.

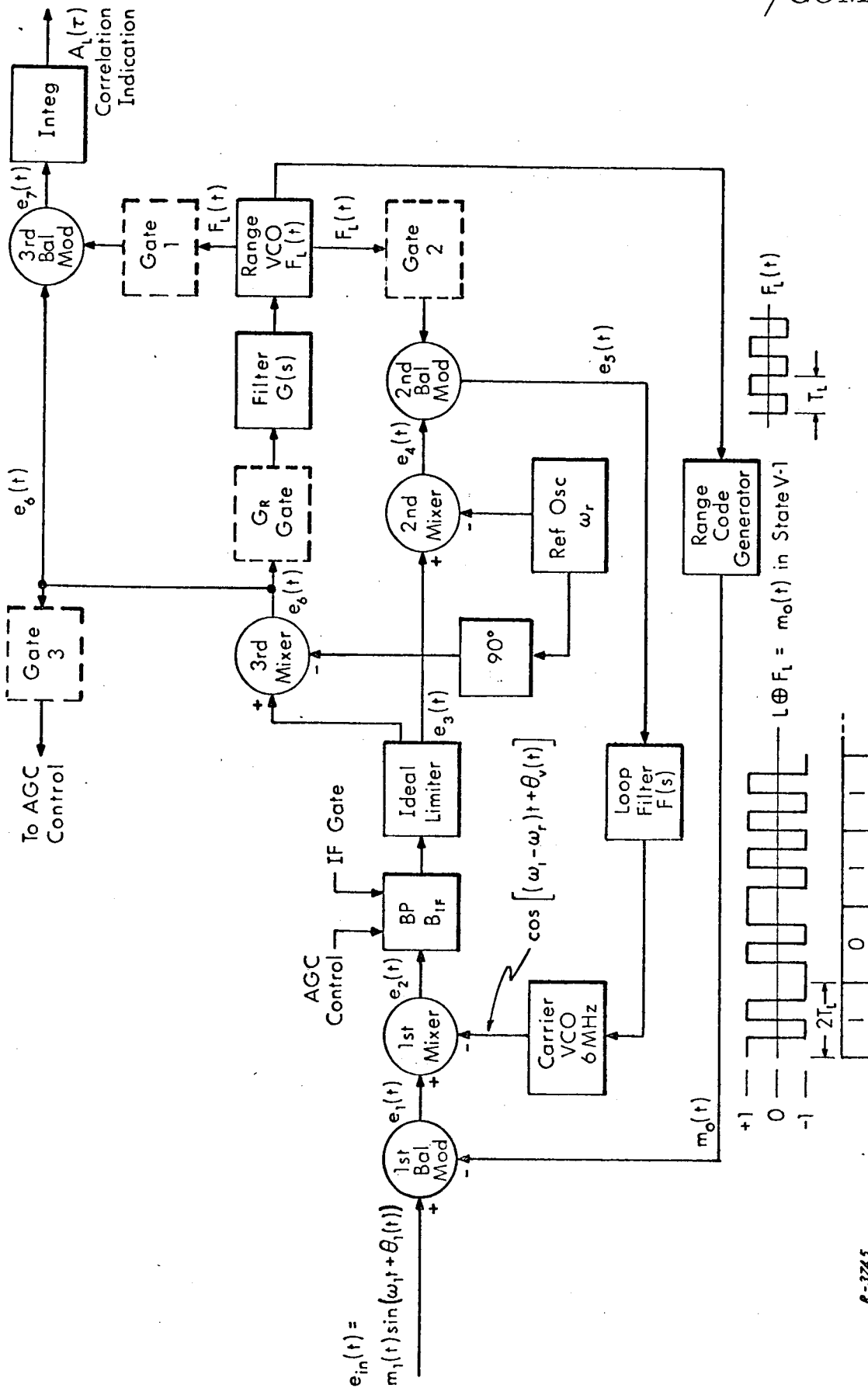


Fig. 11 VTR Carrier and Range Code Loop

R-3745

The different states in the acquisition procedure are four in number, which we will briefly explain. These states occur in sequence in the initial acquisition of a given transponder.

State V-1

m_1 is the L code, while $m_0(t)$ is the $L \oplus F_L$ combined code (Sec. 2.4). The receiver range and carrier VCO's are set to their free-running frequencies. Next the receiver coder shifts the L code. The shifting is done at the rate of 50 bits/s which gives 20 ms time to the carrier loop to acquire at the correct shift. Note that the above inspection time of 20 ms is equal to the total L code period. Completion of this stage is indicated to the transponder via the VHF link.

State V-2

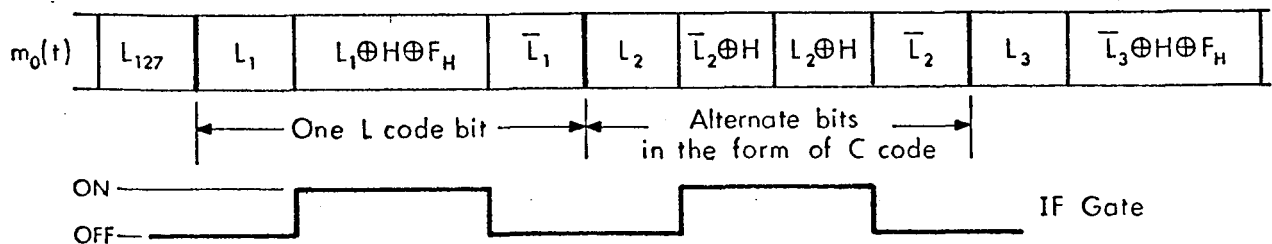
The transponder next removes the reverse doppler linearly at a rate slow enough for the VTR to track the carrier.

State V-3

$m_1(t)$ is now the combined L and H code C (Sec. 2.3), while $m_0(t)$ is changed to $C \oplus F_L$. The H code is now searched over its 511 bits and acquired.

State V-4

$m_0(t)$ is now changed to the following form



R-3746

Note that F_H is a square wave of period equal to the H code bit length. This state is the tracking state. The alternate bits of the L code are combined differently. The combination $L \oplus H \oplus F_H$ is used for carrier tracking while $L \oplus H \oplus F_L$ is

used for code tracking; that is, carrier and range tracking signals are time multiplexed. Synchronized gating for this multiplexed arrangement is in all "paths" of the VTR. A further system complexity is an IF-Gate synchronized to $m_o(t)$ as shown above. This gate cuts off the IF amplifying chain half the time, removing the unused L code. In the event H-code synchronization is lost, this arrangement allows to reverting to state V-3 and continuing L-code tracking.

It should be noted that in the present AROD configuration a two-mode AGC is employed. During the track mode a coherent AGC is used while in the acquisition mode a noncoherent AGC is employed, the object of the noncoherent AGC being to constrain the carrier loop bandwidth to a design maximum. The filter time constants of the AGC in both modes are the same, however.

In the next sections we analyze the acquisition states V-1 and V-3 to determine the nature of the following observations in experiments conducted by Motorola:

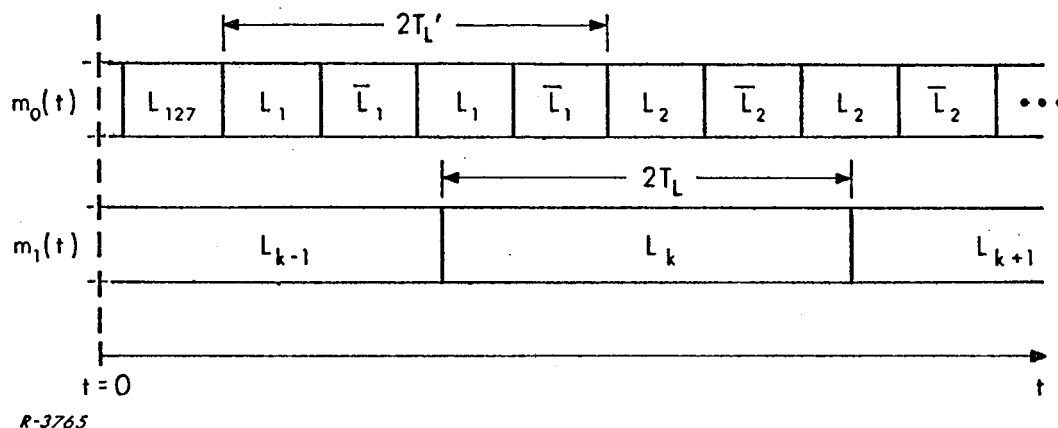
- (1) In acquisition state V-1, and under strong signal conditions, the L-code acquisition detector was falsely triggered by the code noise to temporarily indicate code lock. This lengthened the time to successful acquisition. The introduction of noncoherent AGC reduced the likelihood of this false lock, but did not eliminate it. It was finally eliminated by raising the L-code acquisition threshold A_L by about 2 dB. This amounted to a degradation of the system threshold by 2 dB, from -130 dB into -128 dBm (approximately).
- (2) In acquisition state V-3, if the H-code search termination is disabled, then the VTR correlation indicator (CAD) output is the correlation function of the combined code $C(t)$. It was observed that the actual output of CAD differed from expected correlation function. The observed correlation function had fluctuations as high as 28 dB below peak, i. e., a ratio in $A_L(\tau)$ of 25:1.

3.2 Acquisition State V-1

In this section we will briefly outline the relationships in the VTR during L-code acquisition; this will lead to expressions showing the effect of the

carrier loop phase transfer function. If the two-sided bandwidth of the carrier loop is wider than 100 Hz, it filters out some of the code (Sec. 2.2), so that the receiver does not function as a true cross-correlator. Since the carrier loop noise-bandwidth has to be greater than 500 Hz because of acquisition, the loop tracks a large amount of code causing considerable distortion in the resulting cross-correlation function. This is a basic problem in the AROD ranging code and system concept. In this section we attempt to indicate possible simple solutions to the problem.

In state V-1, $m_1(t)$ is the transmitted L code, while $m_0(t)$ is the code $L \oplus F_L$, as shown on the following diagram.



In the above diagram we have denoted the L code bit period in $m_0(t)$ as $2T_L'$ in order to emphasize that initially the bit sync does not exist. However, the doppler on the L code is less than one Hz, so that bit sync is achieved quickly once the L code is synchronized.

We will now briefly consider the various relationships around the VTR in the absence of noise. This is not a major simplification since system operation is usually under very high SNR, so that independent evaluation of the noise effects for the carrier loop and the range loop in terms of rms phase is a satisfactory estimate of their noise performance.³ Thus, the input signal is

$$e_s(t) = m_1(t) \sin(\omega_1 t + \theta_1(t)) \quad (10)$$

Assuming further that the received and receiver generated bit rates are synchronized we have initially

$$m_o(t) = m_1(t + \tau) F_L(t + \tau) \quad (11)$$

where τ is the initial misalignment of the L code, while $F_L(t + \tau)$ is the actual waveform for the Boolean binary code F_L . The balanced modulator output $e_1(t)$ is then

$$e_1(t) = m_1(t)m_1(t + \tau)F_L(t + \tau)\sin(\omega_1 t + \theta_1(t)) \quad (12)$$

This is mixed down to the reference oscillator frequency ω_r by the carrier VCO whose output is

$$e_v(t) = \cos[(\omega_1 - \omega_r)t + \theta_v(t)] \quad (13)$$

where $(\omega_1 - \omega_r)/2\pi = 6$ MHz is the carrier VCO free-running frequency, and $\theta_v(t)$ is a time varying phase. The first mixer output is therefore

$$e_2(t) = m_1(t)m_1(t + \tau)F_L(t + \tau)\sin[\omega_r t + \theta_1(t) - \theta_v(t)] \quad (14)$$

The effect of the bandpass filter in the IF will be negligible on this signal, so that after mixing down with the reference frequency ω_r we get the second mixer output

$$e_4(t) = m_1(t)m_1(t + \tau)F_L(t + \tau)\sin[\theta_1(t) - \theta_v(t)] \quad (15)$$

The range VCO output $F_L(t + \tau)$ when multiplied to $e_4(t)$ in the second balanced modulator gives

$$e_5(t) = m_1(t)m_1(t + \tau)\sin[\theta_1(t) - \theta_v(t)] \quad (16)$$

which may also be written as

$$\begin{aligned} e_5(t) &= \cos\left[\theta_1(t) - \frac{\pi}{2} m_1(t)m_1(t + \tau) - \theta_v(t)\right] \\ &= \sin\left[\theta_1(t) + \frac{\pi}{2} - \frac{\pi}{2} m_1(t)m_1(t + \tau) - \theta_v(t)\right] \end{aligned} \quad (17)$$

The above is the sinusoidal error term of the carrier phase-locked loop. If the carrier loop is tracking then the linearized phase-transfer model for the loop may be used. The carrier loop transfer function is (Ref. 1, p. 3-31)

$$\frac{\theta_v(t)}{\theta_{in}(t)} = H(s) = \frac{1 + \tau_2 s}{1 + \left[\tau_2 + \frac{1}{G} \right] s + \frac{\tau_1}{G} s^2} \quad (18)$$

where G is the loop gain and, τ_1 and τ_2 are the loop filter time constants. The input phase variation

$$\theta_{in}(t) = \theta_1(t) + \frac{\pi}{2} - \frac{\pi}{2} m_1(t)m_1(t + \tau) \quad (19)$$

hence in operational notation* $\theta_v(t)$ is

$$\theta_v(t) = H(s)\theta_1(t) + \frac{\pi}{2} - \frac{\pi}{2} H(s)(m_1(t)m_1(t + \tau)) \quad (20)$$

Thus we see that if the bandwidth of $H(s)$ is very narrow compared to the significant frequency components of $m_1(t)m_1(t + \tau)$ then

$$\theta_v(t) \approx H(s)\theta_1(t) + \frac{\pi}{2} \quad (21)$$

To observe that the system mechanizes a cross-correlation in this ideal case we get first the output of the quadrature mixer $e_6(t)$ which is

$$e_6(t) = m_1(t)m_1(t + \tau)F_L(t + \tau)\cos[\theta_1(t) - \theta_v(t)] \quad (22)$$

The product of $e_6(t)$ and $F_L(t + \tau)$ is the output $e_7(t)$ of the third balanced modulator (the gates 1 and 2 are on in this stage)

$$e_7(t) = \sin\left[\theta_1(t) - \theta_v(t) + \frac{\pi}{2} m_1(t)m_1(t + \tau)\right] \quad (23)$$

* The operator $H(s)$ will be assumed to operate on all time functions in front of it. One could just as well use the impulse response function and denote the operation as convolution.

Substituting from Eq. (19) for $\theta_v(t)$ we get

$$e_7(t) = \sin \left[\left(1 - H(s) \right) \theta_1(t) + \frac{\pi}{2} \left(1 + H(s) \right) m_1(t) m_1(t + \tau) - \frac{\pi}{2} \right]^* \quad (24)$$

if $H(s)$ does not filter a significant amount of the code product $m_1(t) m_1(t + \tau)$ then

$$e_7(t) \approx m_1(t) m_1(t + \tau) \cos \left[\left(1 - H(s) \right) \theta_1(t) \right] \quad (25)$$

Further, since the carrier loop is to track out the doppler variation $\theta_1(t)$

$$e_7(t) \approx m_1(t) m_1(t + \tau) \quad (26)$$

Integration of $e_7(t)$ by a low pass filter gives the correlation output

$$A_L(\tau) = \int_0^T e_7(t) dt \quad (27)$$

where T is the sampling time of 20 ms. If receiver range loop is opened, $A_L(\tau)$ can be plotted experimentally. Figure 12a reproduces such a plot from Ref. 2, while Fig. 12b shows the effect of wide loop bandwidth.

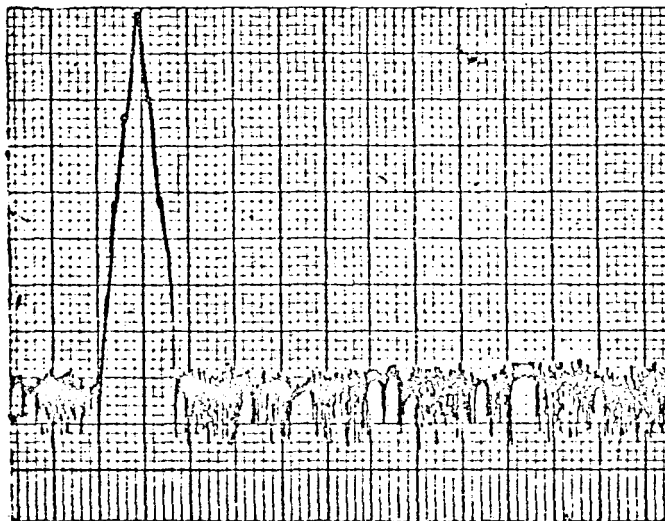
To obtain the analytical form of the correlation output including the carrier loop filtering effect, we go back to Eq. (24). Assuming that the loop tracks the doppler variations $\theta_1(t)$ then

$$e_7(t) \approx \sin \left[\frac{\pi}{2} \left(1 + H(s) \right) m_1(t) m_1(t + \tau) - \frac{\pi}{2} \right] \quad (28)$$

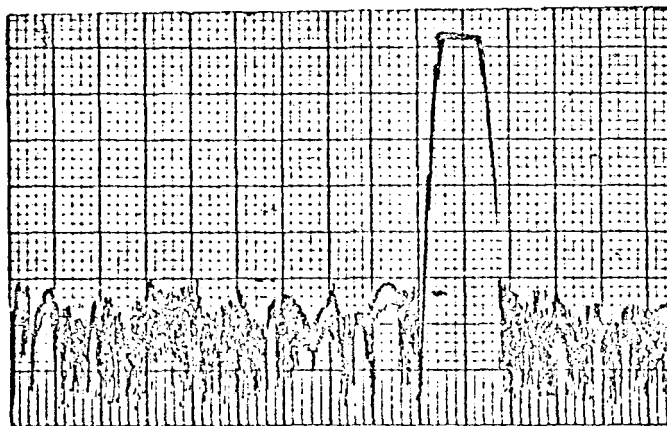
$$\approx m_1(t) m_1(t + \tau) \sin \left(\frac{\pi}{2} H(s) m_1(t) m_1(t + \tau) \right) \quad (29)$$

If the codes are in synchronism $H(s) m_1(t) m_1(t + \tau) = 1$ and therefore the level of $A_L(0)$ is the same as in the case of no code filtering by the carrier loop. It is difficult to see the actual form of $A_L(\tau)$ from $e_7(t)$ above. However, note that in

* Note that $(1 + H(s))$ operation on the code could be changed to $(1 - H(s))$ if $e_6(t)$ is multiplied by -1.



(a) $B_n = 200 \text{ Hz}$



(b) $B_n = 1,133 \text{ Hz}$

Fig. 12. Effect of Carrier Loop Bandwidth on
Correlation Function of L Code
(From Ref. 2 Fig. 15)

$e_7(t)$ the product $m_1(t) m_1(t + \tau)$ is multiplied by the term

$$\sin[(\pi/2) H(s) m_1(t) m_1(t + \tau)]$$

The argument of this sinusoidal term contains only the low frequency components of $m_1(t) m_1(t + \tau)$. Since the peak value of this argument is less than $\pi/2$ rad, it is reasonable to expect this term can be approximated by the first-order FM sidebands. Thus, $e_7(t)$ is very approximately proportional to

$$\{m_1(t) m_1(t + \tau)\} \{k + H(s) m_1(t) m_1(t + \tau)\} \sim e_7(t) \\ k = \text{constant} \quad (30)$$

This is one way of getting a first-order effect of the distortion due to carrier loop filtering. Another approximate manner of looking at this effect is by considering Eq. (28). Using again the approximation that the sinusoidal PM type wave of Eq. (28) is low deviation, then $e_7(t)$ is nearly proportional to

$$(1 + H(s)) m_1(t) m_1(t + \tau) \sim e_7(t) \quad (31)$$

The correlation output would then be

$$A_L(\tau) \sim \int_0^T [1 + H(s)] (m_1(t) m_1(t + \tau)) dt \quad (32)$$

since T equals the period of the code and we can interchange the two linear operations on the product $m_1(t) m_1(t + \tau)$; therefore

$$A_L(\tau) \sim [1 + H(s)]^\dagger \phi_{LL}(\tau) \quad (33)$$

Thus, we see that the distortion in the correlation $A_L(\tau)$ is very approximately due to an additive term containing the low frequency components of the code. The validity of this approximation can only be checked by actual experiment.

An exact solution to the correlation function distortion appears very difficult without significant system changes. Partial alleviation of the problem

[†] In this operation the time variable is τ .

is more likely. The most direct approach being to reduce the carrier loop bandwidth and use either a sweep acquisition aid or sweep the transponder frequency sinusoidally over the range of frequency uncertainty expected (in state V-1).

Another possible solution is pre-filtering of the receiver generated code. Thus, the receiver-coder output would be passed through a filter with a transfer function $T(s)$ so that $m_o(t)$ would become

$$m_o(t) = T(s) [m_1(t + \tau) F_L(t + \tau)] \quad (34)$$

The basis for such an approach is that the carrier loop tracking the code may be looked at as attenuation or amplification of the low frequency components of the code. Thus, if these components are pre-filtered sufficiently, they should be able to compensate for the loop filtering. The actual transfer function may have to be obtained by some approximate analysis together with experimental trial and error and computer simulation, since a direct analytical approach does not appear possible. One property of $T(s)$ which may be expected is that it would have a unity transmission for frequencies of the order of the components of $F_L(t)$ so that we could write

$$m_o(t) = F_L(t + \tau) T(s) m_1(t + \tau) \quad (35)$$

that is, $T(s)$ only effects the L code $m_1(t + \tau)$. It is felt that this approach has considerable potential. However, it will also require studying the effect on the IF Gating employed in the system in state V-4.

3.3 Acquisition State V-3

In acquisition state V-3 the receiver generated code and received code are shown below. If states V-1 and V-2 are satisfactorily completed, the L codes should be in synchronism in this diagram.

$m_1(t)$	L_1	$L_1 \oplus H$	L_1	L_2	$L_2 \oplus H$	L_2	
----------	-------	----------------	-------	-------	----------------	-------	--

$m_0(t)$	L_k	$L_k \oplus H \oplus F_L$	\overline{L}_k	L_{k+1}	$L_{k+1} \oplus H \oplus F_L$	\overline{L}_{k+1}	
----------	-------	---------------------------	------------------	-----------	-------------------------------	----------------------	--

R-3756

Now in the output of the A_L detector we would have ideally the auto-correlation function of the combined code $C(t)$ of Sec. 2. Carrier loop filtering should not effect frequency components of the H code; however, distortion of the L code components will still exist. The correlation function of $C(t)$ around $\tau = 0$ showed in Sec. 2 to be composed of a triangle due to the L code and another narrower one due to the H code. The H code part of the triangle will not be effected by the carrier loop filtering. The L code triangle was, however, in this stage one half the width of the L code correlation function in state V-1. Consequently it appears that in this stage there will be less distortion of the triangle of the L code than shown in Fig. 12.

Experimental results by Motorola indicate such distortion of the output $A_L(\tau)$. The measurements gave minor peaks of the correlation function which are only 28 dB below. These could conceivably lead to temporary false H code lock in the presence of noise.

In Sec. 2 we found that the correlation function of $C(t)$ contains two additional peaks at $\tau = \pm 3T_L/2$ which are only 12 dB below the main peak. These peaks should not effect this acquisition stage if the L code is properly synchronized. However, when signal is temporarily lost and reacquisition is attempted without reverting to stage V-1, then the effect of these peaks would need to be checked.

4. ATMOSPHERIC PROPAGATION EFFECTS ON AROD RANGING ERRORS

4.1 Introduction

An uncertainty exists concerning the range measurement error that can be expected due to propagation of the AROD tracking signal through the atmosphere.⁴ Bounds on the magnitudes of these errors must be determined in order to ascertain the overall AROD system range measurement accuracy. In addition to establishing bounds on the errors, it may be desirable to derive gross corrections for propagation errors which could be applied to actual range measurements. This section is devoted to establishing approximate bounds to these errors, and to an exploration of the merits of gross range corrections.

4.2 The Propagation Effects

In a range (and range-rate) tracking system that depends on the accurate measurement of time (or phase) differences between transmitted and received signals, the principal atmospheric propagation effects resulting in errors are those that introduce extraneous time delays (or phase) shifts, which do not correspond to the round trip straight-line distance between satellite and tracking station. There are two basic types of propagation anomalies that can result in such errors: refraction effects, and multipath or scatter effects. These effects take place in propagation through both the ionospheric and tropospheric regions of the atmosphere.

Refraction effects are due to the variation of propagation velocity in the different layers of the earth's atmosphere. This variation results in two effects which are sometimes considered separately:

- (a) a bending of the ray, which amounts to a lengthening of the path of propagation, and
- (b) a slowing down of the ray, which results in an added extraneous time delay (or phase shift).

The total time delays (or phase shifts) are strongly dependent on the angle of elevation of the vehicle, because a smaller angle of elevation implies a longer distance to be travelled by the radio wave through the atmosphere. Delays due to refraction can be appreciable and are quite stable in general, changing slowly as the vehicle changes its elevation with respect to the ground station, and with diurnal changes in the propagation velocity in the various layers of the atmosphere. These delays are also dependent on the frequency of the radiated waves. Adequate compensation of the ranging errors caused by the refraction effects can be implemented, provided that accurate analytical relations between range errors and pertinent parameters are available.

Multipath or scatter effects are due to turbulence and time-varying irregularities in the structure and composition of the atmosphere. They result in rapid randomly varying time delay (or phase shifts), as well as in rapid random fluctuations in the received signal amplitude. The delay fluctuations are strongly dependent on frequency. Amplitude changes could result in system failure, if the signal-to-noise ratio at the input to a receiver drops below the detection threshold. We will not be concerned here with this possibility, however, on the assumption that adequate transmitted power levels have been designed into the system. The range errors caused by the scatter effects cannot be adequately compensated, because of the complexity of the relations between the error and the pertinent parameters (if known), and the rapid random fluctuation nature of the errors.

4.3 Review of Some Previous Findings

Extensive studies have been conducted in the past in the area of effects of propagation anomalies on the accuracy of tracking systems. We review here some of the pertinent findings.

One of the more pertinent research efforts in this area was conducted by Philco Research Division.⁵ This study was partly concerned with the

constant (or diurnally varying) range errors caused by the ionospheric and tropospheric refraction effects. These errors are computed as a function of frequency, for two specific angles of elevation: 5° and 90° . A model for the dependence of the refractive index on altitude in a spherically-symmetric atmosphere is assumed. In the troposphere the refractive index is assumed to vary exponentially; while in the ionosphere a weighted average of various models proposed in the literature was assumed.

At S-band, the band associated with most range and range-rate systems, the static range error amounts to +120 feet (daytime) and +90 feet (nighttime) for a vehicle at altitude greater than 1000 n.m. and an elevation angle of 5° , (so that the vehicle is well outside the earth's atmosphere and is thus suffering the maximum error). For an elevation angle of 90° , the corresponding numbers are +25 feet and +12 feet respectively. Of this total range error, most of the contribution (70 to 80 percent) arises from the troposphere for small elevation angles, and a lesser percentage for high elevation angles. Note that these errors cannot be "calibrated out" because they are not fixed errors.

These computed errors may vary ± 50 percent, depending upon local conditions, weather and season. Much of this uncertainty, including the diurnal variations, can be resolved from a knowledge of the refractive index at the tracking station, so that predictions about the error can be computed as often as desired in order to make corrections of the range data. However, the fact that the Philco study does not give error estimates as a function of the elevation angle makes it impossible to use its predictions to correct the ranging data from a vehicle that is rapidly and continuously changing its angle of elevation.

Another pertinent study effort was conducted by J. J. Freeman Associates, Inc. in relation to the Goddard Range and Range Rate System.⁶ This study concludes, on the basis of previous experience, that the rms

fluctuations in range error due to scatter effects in the ionosphere and troposphere do not exceed the order of magnitude of one foot.

The study then deals with methods of correcting for the slowly changing errors due to refraction in the troposphere only for a propagation frequency at S-band. It is found that the contribution due to ray bending (see paragraph 2(a) above) is negligible compared to that due to the decreased propagation velocity, for elevations greater than about 4° . It goes on to compute an exact expression for the error as a function of the angle of elevation, as well as an approximate expression in which the bending of the ray is neglected, all on the basis of a CRPL exponential reference atmosphere.

It is then suggested that the approximate expression, augmented by frequent measurements of the index of refraction at the tracking station, be used to make real time corrections of the ranging information. It is proposed to make an estimate of the rms difference between predicted and actual range errors, in order to justify the utility of making the corrections. However, no conclusive results are achieved concerning this residual error after correction.

4.4 Ranging Errors From Tropospheric Propagation

This section presents a simple and approximate bound on the range error caused by propagation through the troposphere. The vehicle is assumed to be at a great altitude, which means practically "several hundred miles." At lower altitude the error will be less than this bound.

Consider a plane earth with refractive index, $n(y)$, a function only of the altitude y (see Fig. 13). The inclination β of the propagation direction to the horizontal at any height y is given by

$$n(y) \sin \beta(y) = \text{const.} = \sin \beta_0 \quad (36)$$

where β_0 is the true elevation angle of the vehicle at the ground station.

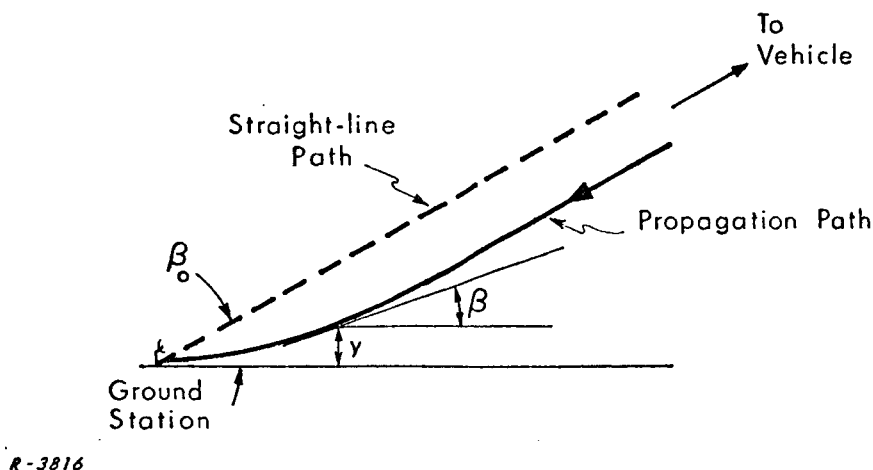


Fig. 13 Refractive Propagation through the Troposphere

The lengthening of the propagation path is given by

$$\begin{aligned}\Delta L &= \int \left\{ \frac{1}{\sin \beta(y)} - \frac{1}{\sin \beta_0} \right\} dy \\ &= \int \frac{n(y) - 1}{\sin \beta_0} dy\end{aligned}\quad (37)$$

The refractive index at sea level⁷ is normally $n_0 = 1.000324$. Since $(n(y) - 1)$ is effectively proportional to the air density, ρ , throughout its range of significance, we can write

$$n(y) - 1 = 3.24 \times 10^{-4} \frac{\rho(y)}{\rho_0} \quad (38)$$

where ρ_0 is the air density at ground level. Then

$$\Delta L = \frac{3.24 \times 10^{-4}}{\sin \beta_0} \frac{1}{\rho_0} \int \rho(y) dy \quad (39)$$

Utilizing

$$p_0 = g \int_0^\infty \rho(y) dy \quad (40)$$

where

p_o is the atmospheric pressure at ground, assumed constant, and
 g is the gravitational acceleration, also assumed constant,

we get

$$\Delta L = \frac{3.24 \times 10^{-4}}{\sin \beta_o} \frac{p_o}{g \rho_o} \cong \frac{2.55}{\sin \beta_o} \text{ meters} \quad (41)$$

We thus have in Eq. (41) a very simple estimate of the one-way lengthening of the propagation path caused by tropospheric refraction. The estimate is a function only of the elevation angle of the vehicle at the ground station. The two-way path lengthening is simply twice that of Eq. (41).

This is a rather large error, especially at low elevation angles, e. g., 14.6 meters for $\beta_o = 10^\circ$. However, the error can be fairly accurately predicted and compensated. Note that, by the gas law, the factor p_o/ρ_o in Eq. (41) is proportional to the absolute surface air temperature. This result is independent of condition of the atmosphere, except for the assumption of horizontal stratification. It may therefore be stated that for any horizontally stratified atmosphere, the path length correction due to atmospheric refraction is, apart from earth curvature effects, given quite accurately by an expression of the form

$$\Delta L = \frac{A}{\sin \beta_o} \left(\frac{\rho_o}{\rho_s} \right) \left(\frac{T_o}{T_s} \right) \quad (42)$$

where ρ_o and T_o are measured air density and temperature in the neighborhood of the ground antenna, and ρ_s and T_s are standard density and temperature. For reasonable reference values ρ_s and T_s , A is on the order of 2.55 meters. It could be determined with great accuracy. This formula could also be modified to take earth curvature effects into account, very accurately.

Assuming that such a correction is accurately made, the remaining errors are due to horizontal gradients in atmospheric structure. These should

be at least an order of magnitude smaller under usual conditions. Unusual conditions, such as passage of a sharp cold front, would certainly be known, and could be compensated for. It seems very likely that these compensation processes if carefully carried out could reduce final range error to less than 0.1 meter as long as $\beta_1 > 10^\circ$.

4.5 Ranging Errors from Ionospheric Propagation

This section presents a simple and approximate bound on the steady part of the range error caused by propagation through the ionosphere.

The group velocity at any point in the ionosphere is

$$v_g = c \sqrt{1 - \frac{f_c^2}{f^2}} \quad (43)$$

where

$$\begin{aligned} c &= \text{velocity of light,} \\ f_c &= 8.1 N \times 10^7, \\ N &= \text{free electrons/cm}^3, \text{ and} \\ f &= \text{frequency in Hz.} \end{aligned}$$

For vertical traversal of the total ionosphere, the lengthening of the propagation path is

$$\begin{aligned} (\Delta L)_{\text{vert}} &= \int \left\{ 1 - \sqrt{1 - \frac{f_c^2}{f^2}} \right\} dy \\ &\approx \int \frac{f_c^2}{2f^2} dy = \frac{8.1 \times 10^7}{2f^2} \int_{\text{vert}} N(y) dy \end{aligned} \quad (44)$$

For traversal at elevation angle β through a horizontally stratified ionosphere this value is to be multiplied by $1/\sin \beta$. The result thus depends only on β and on the integrated electron density, represented by the integral in Eq. (44).

This line of investigation has been exploited fully in Ref. 8. Typical values for $f = 2$ GHz work out to be

$$\Delta L = \frac{0.96}{\sin \beta} \text{ meters} \quad (45)$$

The two-way path lengthening is, of course, simply twice that of Eq. (45).

Although ionospheric structure changes conspicuously with time of day, season, etc., the integrated electron density is one of the more stable parameters. The error could probably be reduced by a factor of 4 or 5 by a uniform correction of the form $B/\sin \beta$ where the constant B is carefully chosen. An additional factor of 2 or 3 could probably be gained by programming B to follow a typical diurnal and seasonal curve. Of course, if the vertical integrated electron density is more accurately predicted or directly measured, very precise compensation could be made in principle, but this would appear very difficult.

The doppler frequency is not falsified by these effects for a vehicle above the ionosphere.

Because of the appearance of $1/\sin \beta$ in the correction formulae (Eqs. (41) and (45)), it is clear that any compensation could be performed on the ground, and inserted as update data in the range data extraction unit.

These compensation schemes involve undesirable complications. It might be easier to make use of the fact that all types of error are of the form $K/\sin \beta$ where K is perhaps a difficult number to derive a priori, but may be taken as constant at least on one vehicle passage. From trajectory dynamics or from comparison with doppler velocity measurements, an adequate estimate of K may be made periodically.

5. POSITION DETERMINATION WITH THE AROD SYSTEM

5.1 Introduction

An area of proposed future equipment development in the evolution of the AROD system is that of a vehicle-borne computer which will transform AROD tracking measurements into parameters representing the vehicle velocity and the position of the vehicle in space. One of the first steps in determining vehicle-borne computer requirements for the AROD system is a decision as to the coordinate system in which position computation will be performed. A three-dimension cartesian coordinate system with center in the vicinity of AROD ground stations permits on-board position fixing computations by algebraic manipulation of measured distances obtained from the AROD system and pre-inserted station coordinate information. Vehicle-borne computer trigonometric expansions are not required for the mathematics involved in a rectangular coordinate system (thus resulting in reduced computer complexity and weight, and on-board power required), and the vehicle position is determined with reference to the cartesian coordinate system center.

Since the pertinent measured parameters in the AROD system are the distances from the vehicle to each of three ground stations,* the positions of these ground stations relative to the cartesian system center must be known. This relative position information can be computed in advance of the vehicle launch and stored in the vehicle system memory. The computation process consists of conversion of ground station coordinates referred to an earth-center coordinate system to the cartesian system of the vehicle-borne computer.

During the course of translation of station coordinates for various stations to the coordinate system of the vehicle-borne computer, questions arose

*Distance information to four ground stations is available when all stations are acquired. For this simplified treatise, however, only a three-station fix will be considered.

concerning the exact meaning and accuracies of the coordinates given. This section will therefore first deal with geodetic terminology and the basics and meaning of geodetic measurements as related to AROD system fixing. The mathematics for translation of ground station coordinates to the vehicle-borne computer cartesian system will be treated next. Finally, the mathematical process of vehicle position determination from cartesian station coordinates and AROD system measurements will be covered, with a qualitative discussion of expected errors.

5.2 Geodetic Considerations

Accurate knowledge of the position of AROD ground stations is paramount to the precision fixing of a vehicle in space. An understanding of the various earth-center coordinate systems and how they relate to the cartesian coordinate system proposed for the vehicle computer is therefore necessary. This section will be concerned with the establishment of the relationship between these coordinate systems, but will not attempt to be rigorous in the treatment of this subject.*

5.2.1 Reference Surfaces

There are three different reference surfaces used by geodesists in determining positions on earth (see Fig. 14). It is necessary to distinguish between these reference surfaces, since each plays an important part in the development of geodetic control.

The first, the earth's topographic surface is irregular with its variety of land forms, mountains, valleys, and ocean depths; yet its features can be delineated, and it is, in fact, the surface on which geodetic measurements are actually made.

* A more complete discussion of the elements of geodesy as applied to tracking systems may be found in Ref. 1, from which this text is synopsized.

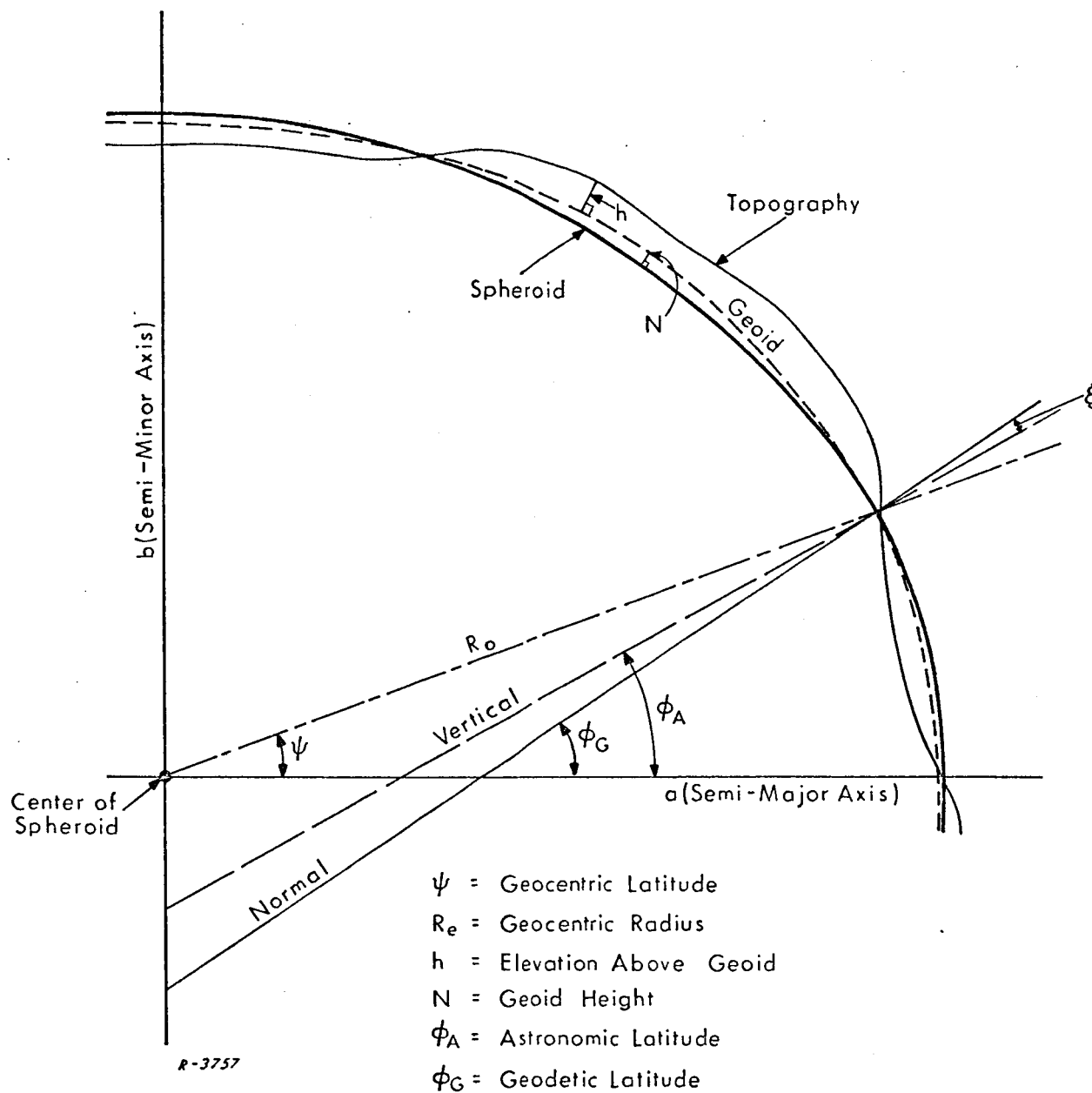


Fig. 14 Meridional Section (From Ref. 9)

The geodesist, however, reduces his measurements (and refers his observations) to the geoid. The geoid is an equipotential surface of gravity, everywhere normal to the gravity vector, which coincides with the smooth but undulated surface to which the waters of the earth would adjust, free of disturbing forces, and which may be imagined to extend through the continents. The geoid, the best reference surface available, is represented by mean sea level, and it is the purpose of horizontal geodetic surveys to determine on the geoid, positions of the projections (along the local vertical) of points lying on the earth's surface, above or below the geoid. A vertical survey determines the distance along the local vertical from points on the earth's surface to mean sea level. Due to the complex distribution of earth crustal materials and the irregular masses of varied densities below the surface, the gravitational force varies from place to place, not only in amount but in direction. Rarely does the local center of gravity vector pass through the geometric center of the earth.

The forces that deflect the gravity vector act as well on sea level, causing it to display a warped surface. To avoid the problems of exact position determination on this non-mathematical figure, computations are normally made on a spheroid deduced as the geometrical figure which best fits the geoid or some portion of it. The spheroid is defined by two numbers, the length of the semi-major and semi-minor axes (or semi-major axis and a ratio called "flattening") which assign both size and mathematical shape to the surface. Since the spheroid is a regular surface it does not coincide with the geoid, and the areas of separation are known as geoid heights or geoid separations. There is no way to measure the geoid separation directly, though sufficient geodetic data may permit a good estimation of it. This limitation interferes with the establishment of completely accurate survey datums.

Several increasingly precise determinations of the dimensions of the best-fitting spheroid have been made; in fact, one of the primary elements of

geodesy has been the determination of the size and shape of the earth. The uncertainties in the various dimensions as evidenced by the several spheroids in use around the world today illustrate the difficulty in the problem of determining the relative positions of tracking stations. Sea level itself, the best reference surface, is only an approximation, since there are many dynamic effects, both long and short term, that modify this surface.

5.2.2 Geodetic Surveys

Geodetic surveys are those which take into consideration the curvature of the earth. Within the limits that a given spheroid is used to define the shape of the earth, distances and angles over the earth's surface can be measured, and latitudes, longitudes, and azimuths computed which will be accurate relative to each other. Positions from geodetic surveys are known as geodetic positions and must be used whenever accurate relative distances and directions are desired. It should be made clear that insofar as relative distance within the coverage of the geodetic net is concerned, no errors other than the mechanical errors of measurement are involved. Geodetic positions being the result of measurements made on the surface of the earth, if a different spheroid were used, all the positions and azimuths would be redefined but the relative distances would remain unchanged.

Horizontal Positioning

Four surveying techniques are in general use for determining positions on the earth's surface: astronomic positioning, triangulation, triaterlation, and traverse. In recent years, technological developments have added several new methods utilizing celestial techniques.

Astronomical observations are made with optical instruments containing leveling devices, and when in use the vertical axis of the instrument is made to

coincide with the gravity vector. Since the geoid to which the positions are referenced is an irregular, non-mathematical surface, however, and distances are not measured, positions observed some distance apart are wholly independent of each other. The calculated distance and azimuth between them cannot, therefore, be expected to agree with actual horizontal survey results.

Triangulation also involves the use of optical instruments in which the vertical axis coincides with the local gravity vector. In this system the base line is measured directly, all other distances being derived by angle measurements of triangles and trigonometric calculation. The accuracy with which a distant station may be located is nearly independent of the character of the intervening country, since the ground between stations does not have to be traversed.

Triangulation is a procedure wherein the triangle sides are measured directly, frequently over long distances (to 500 miles) with electronic distance measuring equipment. Angles are calculated trigonometrically and geodetic positions determined relative to an origin, as in conventional triangulation.

Traverse, the simplest means of extending control, involves the measurement of angles and distances between a number of intervisible survey points. These measurements are generally made by conventional optical instruments, and tapes or electronic distance measuring equipments, and the position of each control point computed relative to the origin from the measured data.

In celestial techniques, a visible target such as the moon or a satellite (the position of which is known) is observed against a star background. The coordinates of a point on the earth are determined through the observed relationship of the target in space to the star background. The principal advantage of this survey method is that it eliminates the effect of local gravity deflection, since verticality of the observing instrument is not a factor. Although gaining acceptance, this method has not been widely used operationally, pending resolution of certain problems inherent in the technique.

Vertical Positioning

Vertical control is normally extended by one of three techniques: differential, trigonometric, and barometric leveling.

An optical device whose vertical axis is coincident with the gravity vector is used in differential leveling. Readings are made through a telescope normal to the vertical axis on each of two upright graduated staffs, and the difference between readings represents the difference in elevation of their bases.

Trigonometric leveling involves the measurement of a vertical angle and horizontal distance. By solution of the resulting right triangle, the difference in elevation may be calculated. The accuracy of this method is affected greatly by vertical optical refraction.

Barometric leveling, the least precise of the three methods, employs instruments calibrated to measure the barometric pressure difference between two sites. This difference in pressure is converted to an elevation difference.

Geodetic Datums

Geodetic control requires two types of datums: a horizontal datum which forms a basis for the computation of horizontal control surveys in which the curvature of the earth is considered, and a vertical datum to which elevation is referred.

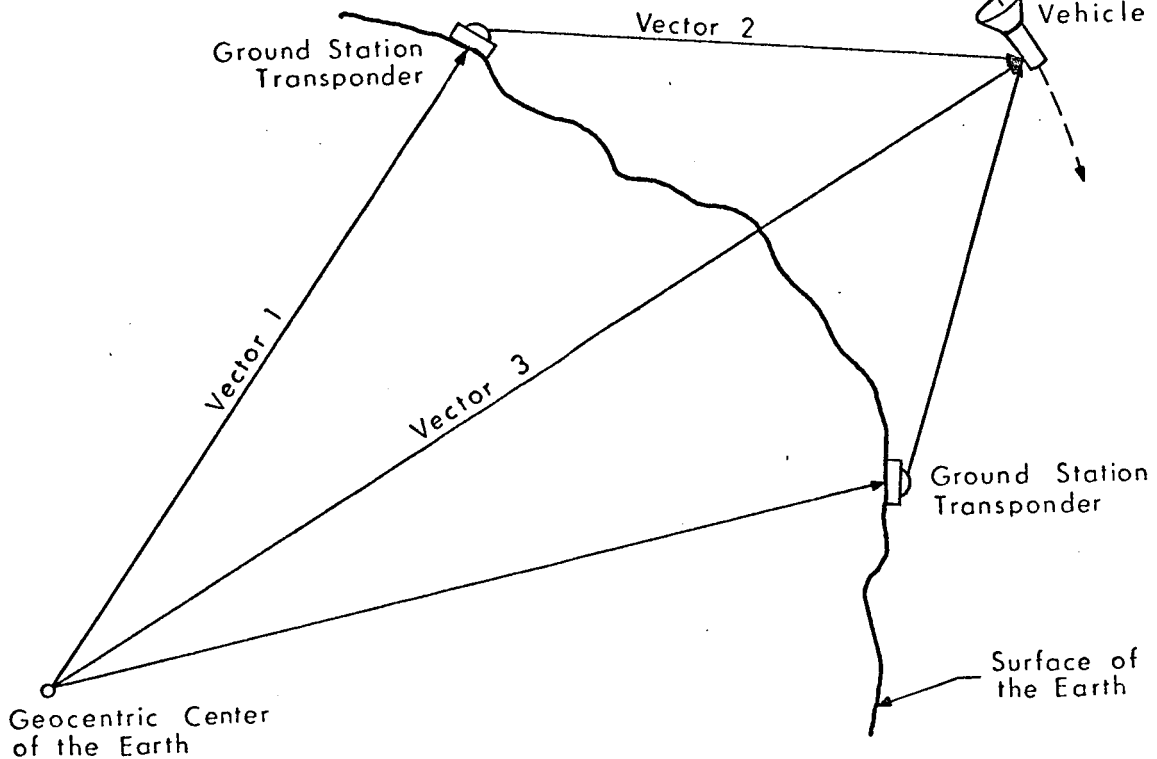
A horizontal geodetic datum has been traditionally defined by five quantities: the lengths of the semi-major and semi-minor axes (or by a ratio, flattening) of its spheroid; an azimuth from its point of origin to another point; and the latitude and longitude of the point of origin. It should be noted, however, that knowledge of the deflection of the vertical at the point of origin is a prerequisite to an improved geodetic datum.

A change in any of these established quantities or in the assumption regarding deflection, will result in a change in the computed coordinates of any point based on the datum defined. Thus, there will be a basic lack of conformity in position, distance, and azimuth derived from geodetic surveys having points in common but based on different datums.

The full definition of position includes the third dimension, height. It has long been recognized that the use of geocentric distances would be desirable as a means of avoiding the uncertain factor of geoid separation (see Fig. 14). For several reasons this is not a convenient system. The origin is inaccessible, and instruments cannot be oriented to it. Its position must be deduced from multiple observations. Thus, as a practical matter, elevations are generally referred to mean sea level or the geoid. As in interconnections of horizontal datums, ties between vertical datums reveal many discrepancies, as sea level is an approximation affected by tides, winds and currents that displace the waters unnaturally. Development of the datum over a survey area is further complicated by continental instability, and the fact that the total volume of sea water seems to vary with time.

5.2.3 Application to Space Tracking Operations

A world tracking range such as the Manned Space Flight Network is typified in part by Fig. 15. If the geocentric distance and angles of the vehicle, and the changes in these parameters with respect to time, could be measured directly from the earth's geocentric center, tracking would be relatively simple. Unfortunately, however, vehicle position and velocity measurements must be made from the ground station transponder on the earth's topographic surface, using our best knowledge of vector 1 and the measured vector 2. The problem of determining vector 1 consists of the summation of the following factors: the



R-3758

Fig. 15 Vectors Involved in Position Determination of Space Vehicles

geoidal separation estimated by the geodesist, using somewhat involved procedures which will not be covered in this section; the topographic height above the geoid, known from spirit or trigonometric leveling; and the radius of the spheroid at the station. These three factors are summed to yield the geocentric radius of the earth measured from the earth's center to the data point (namely the ground station transponder).

The geocentric angles of vector 1 are known as geocentric latitude and geocentric longitude, and are determined by translation from geodetic coordinates. The translation process is beyond the scope of the discussion in this section, but it will be noted that (in general) the geocentric coordinates are derived from topographic land surveys. It will also be noted that geocentric longitude is the same as geodetic longitude.

The length and rate-of-change of length of vector 2 are determined in the AROD vehicle, and it is thus possible with a knowledge of vector 1 to three or more ground stations, and measured values of vector 2 to these same ground stations, to fix the vehicle in space and determine the velocity vector relative to an earth-center coordinate system. By proper translation, the vehicle may be fixed and the velocity vector determined relative to any coordinate system center.

5.3 In-Flight Computer Coordinate System

The utilization of a rectangular coordinate system for in-flight position computation is convenient for the AROD vehicle-borne computer since, assuming station coordinates in rectangular form relative to the cartesian system center are inserted in the computer memory, only algebraic manipulations are required for vehicle fixing. Such a coordinate system is shown in Fig. 16. The Z axis is a geocentric vertical passing through the coordinate system center (positive values of Z in the direction away from the earth's center). The Y axis intersects the coordinate system center (usually defined at a point near the earth's surface and in close proximity to the ground stations) normal to the Z axis, and is coincident with a plane surface passing through earth North and South poles and the coordinate system center. Positive values of Y are defined in the northerly direction. The X axis is orthogonal to Y and Z axes. Positive values of X are defined in the easterly direction. Stations A, B, and C are defined by vectors \bar{A} , \bar{B} , and \bar{C} , each with components in X, Y, and Z directions. Range measurements from the vehicle to the stations are defined by quantities S_a , S_b , and S_c .

5.4 Station Coordinate Translation

In order to effect a vehicle-borne computer solution to the vehicle position based on range measurements to each of three ground stations, the coordinates of the ground stations relative to some common point must be inserted in

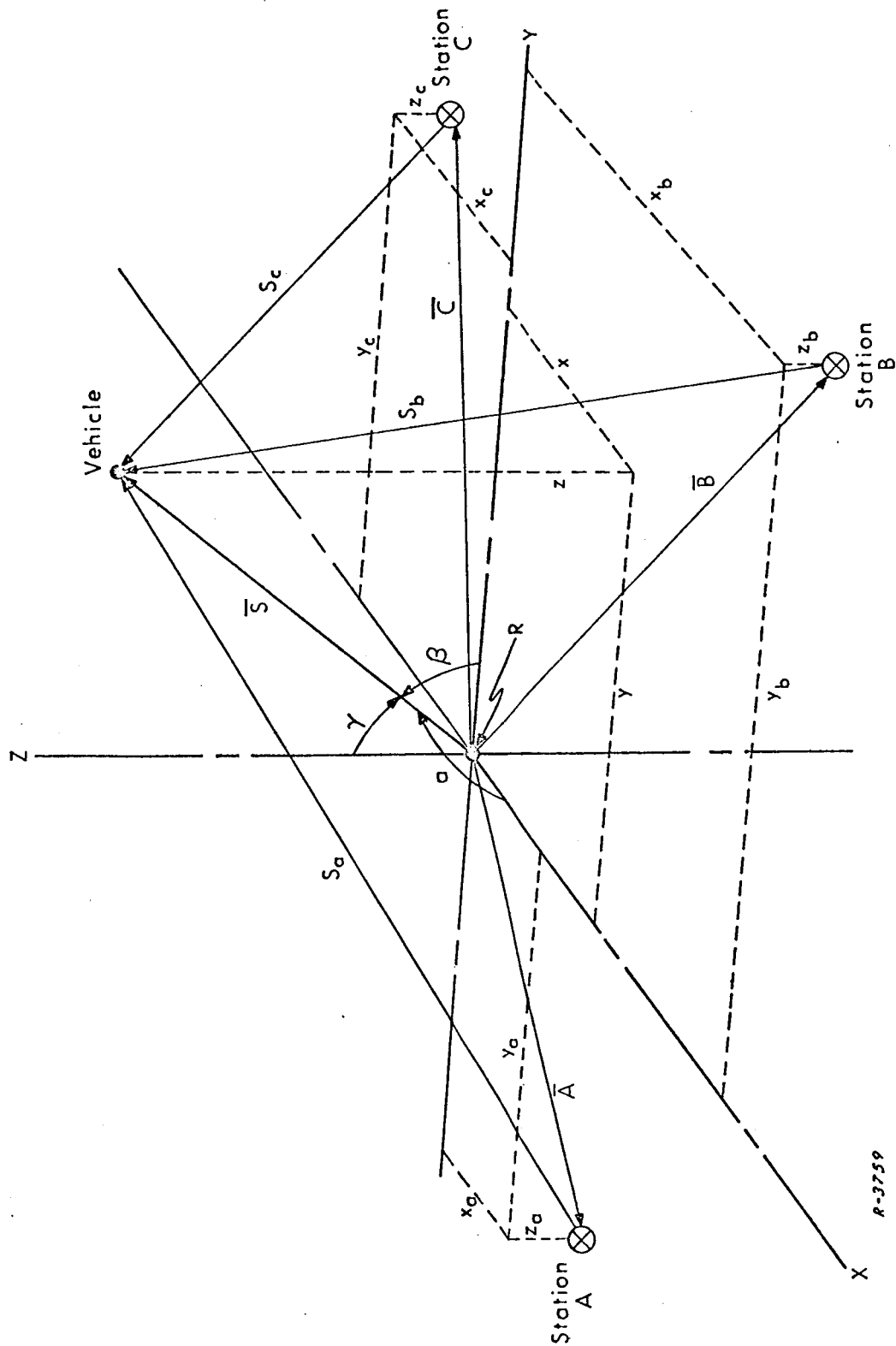


Fig. 16 Computer Coordinate System

R-3759

the computer memory prior to launch. It is most convenient to store these coordinates in linear quantities of the cartesian coordinate system described in Sec. 2. Station coordinates, however, are given (in the most convenient form) in geocentric values. It is thus necessary to translate the station coordinates from their earth-center, polar form into the local-center, cartesian form required for the vehicle computer. This translation is accomplished on the ground prior to vehicle launch. A pictorial of the geometry involved in the translation process is shown in Fig. 17. Note the relationship between the earth-center coordinate system and that system depicted in Fig. 16.

The location of an AROD ground station, and of the computer coordinate system center, is described in the earth-center polar form by three values: two angles and a linear distance. The distance is the geocentric radius of the earth at the exact point of intersection. For example, at Station A the geocentric radius is $|\bar{R}_a|$ or R_a . The two angles which complete the description of the Station A location are ϕ_a and ψ_a , the geocentric longitude and latitude of the station, respectively.

In order to translate the angles and distance representing the station location in the earth-center coordinate system into linear quantities x_a , y_a , and z_a , which describe the station position with respect to the computer coordinate system center, it is necessary to define a series of coordinate systems, through which the earth-center system described above is rotated, in order to derive the rectangular components. The first system defined is shown in Fig. 18. A line through the earth's North/South Poles is defined as the Z''' axis, a line through the earth's center intersecting the Greenwich Meridian at the equator represents the Y''' axis, and a line orthogonal to both Y''' and Z''' axes intersecting the center of the earth represents the X''' axis. Thus, for Station A,

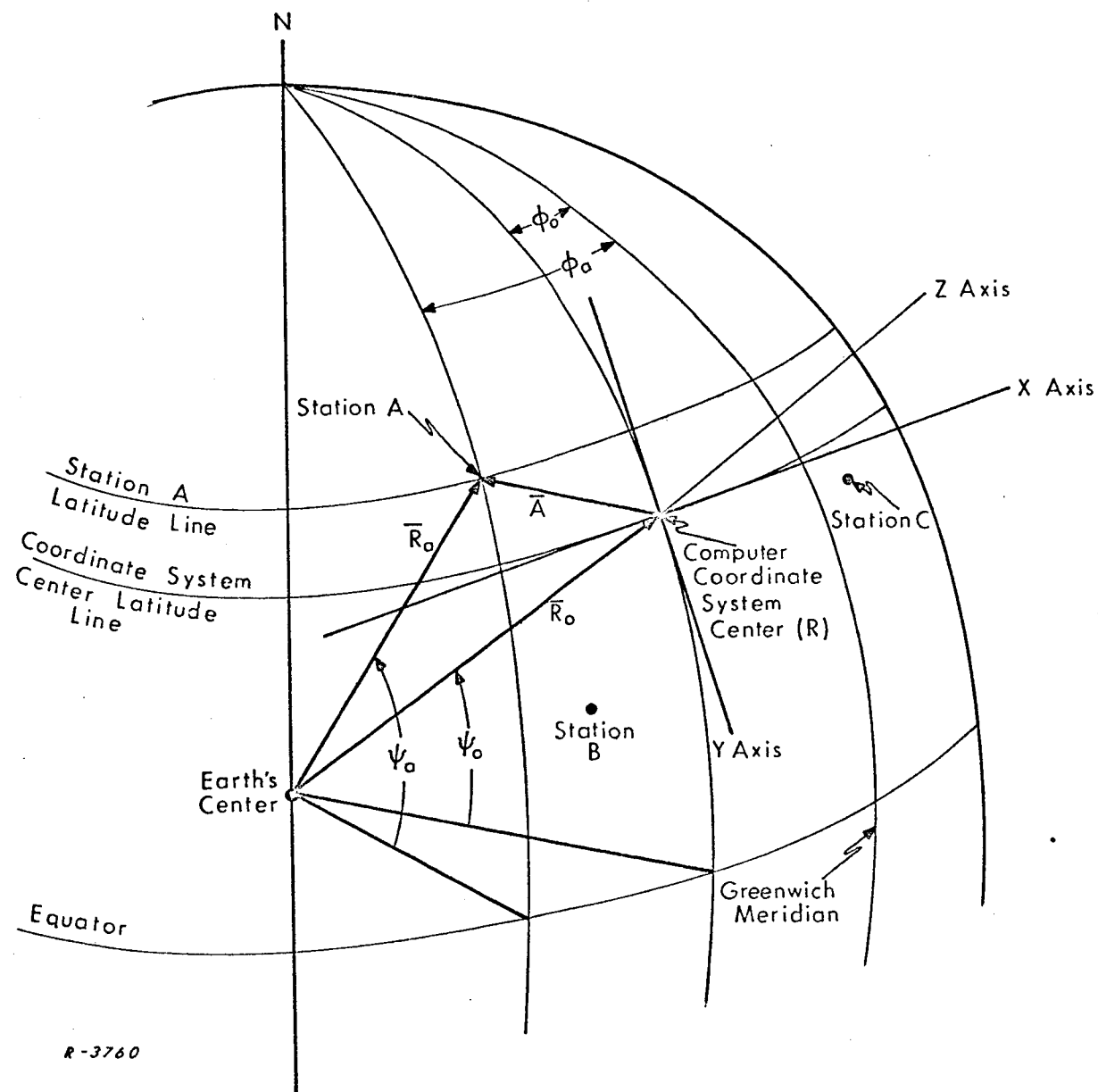
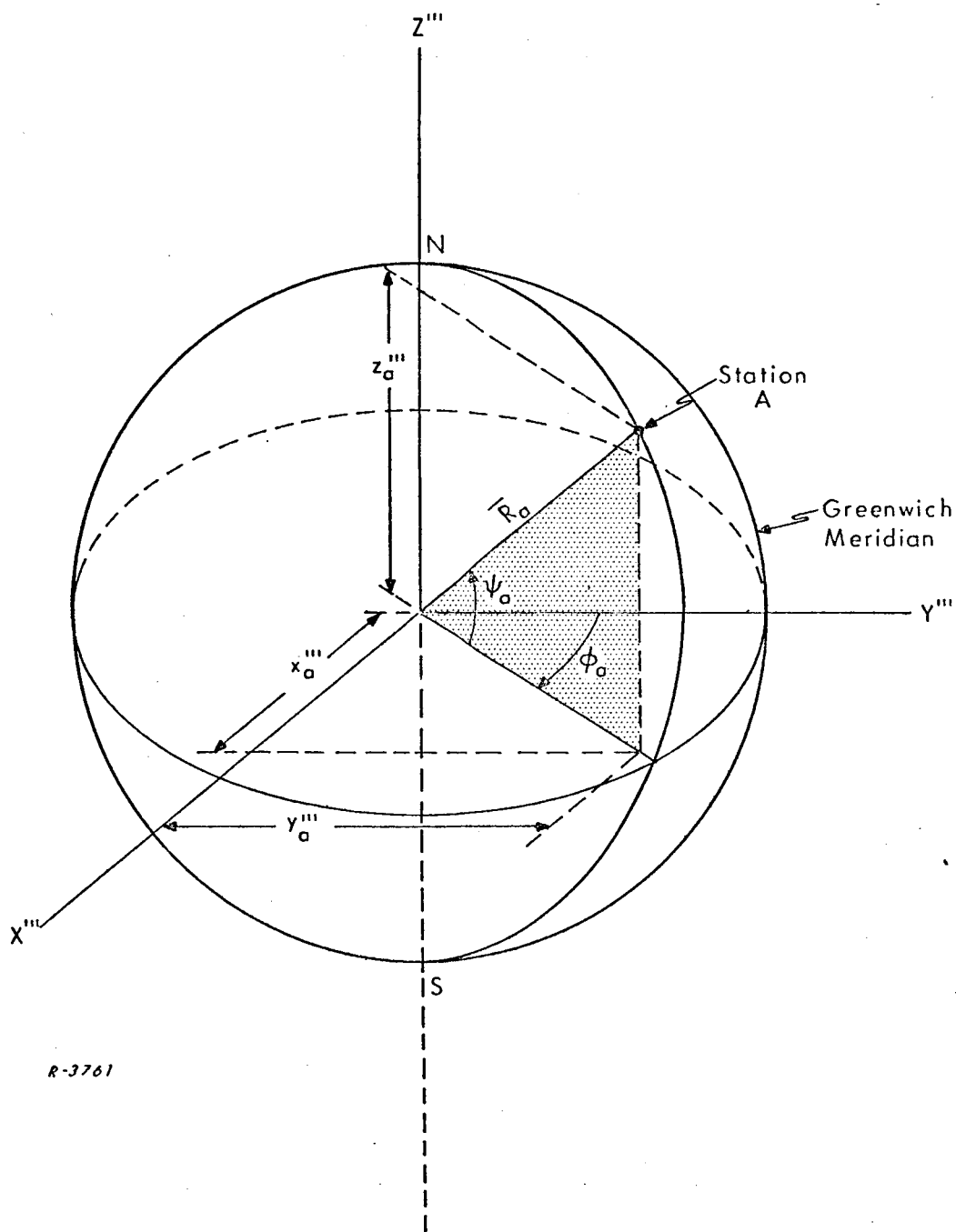


Fig. 17 Geometry of Ground Station Coordinate Translation



R-3761

Fig. 18 Transformation of Station Coordinate to Earth-Center, Rectangular Coordinate System

$$x_a''' = R_a (\cos \psi_a)(\sin \phi_a) \quad (46)$$

$$y_a''' = R_a (\cos \psi_a)(\cos \phi_a) \quad (47)$$

$$z_a''' = R_a \sin \psi_a \quad (48)$$

The quantities x_a''' , y_a''' , and z_a''' describe the location of Station A in a rectangular, earth-center coordinate system. In succeeding steps, these quantities will be translated to linear values in the rectangular coordinate system described in Sec. 5.2.

The next step is to rotate the rectangular system shown in Fig. 18 about axis defined by vector \bar{R}_O (see Fig. 17). Rotating the coordinate system of Fig. 18 through the angle ϕ_O about the Z''' axis (see Fig. 19), a coordinate system is defined wherein:

$$x_a'' = x_a''' \cos \phi_O - y_a''' \sin \phi_O \quad (49)$$

$$y_a'' = x_a''' \sin \phi_O + y_a''' \cos \phi_O \quad (50)$$

$$z_a'' = z_a''' \quad (51)$$

The new coordinate system is next rotated about the X_a'' axis through the angle $(90^\circ - \psi_O)$ as shown in Fig. 20. Thus, a coordinate system is defined where:

$$x_a' = x_a'' \quad (52)$$

$$y_a' = y_a'' \cos (90^\circ - \psi_O) - z_a'' \sin (90^\circ - \psi_O) = y_a'' \sin \psi_O - z_a'' \cos \psi_O \quad (53)$$

$$z_a' = y_a'' \sin (90^\circ - \psi_O) + z_a'' \cos (90^\circ - \psi_O) = y_a'' \cos \psi_O - z_a'' \sin \psi_O \quad (54)$$

The last operation required for the coordinate system translation is that of subtracting out the value of R_O from the Station A rectangular component along the Z axis. In this process, the rectangular components of Eqs. (52) through (54) are

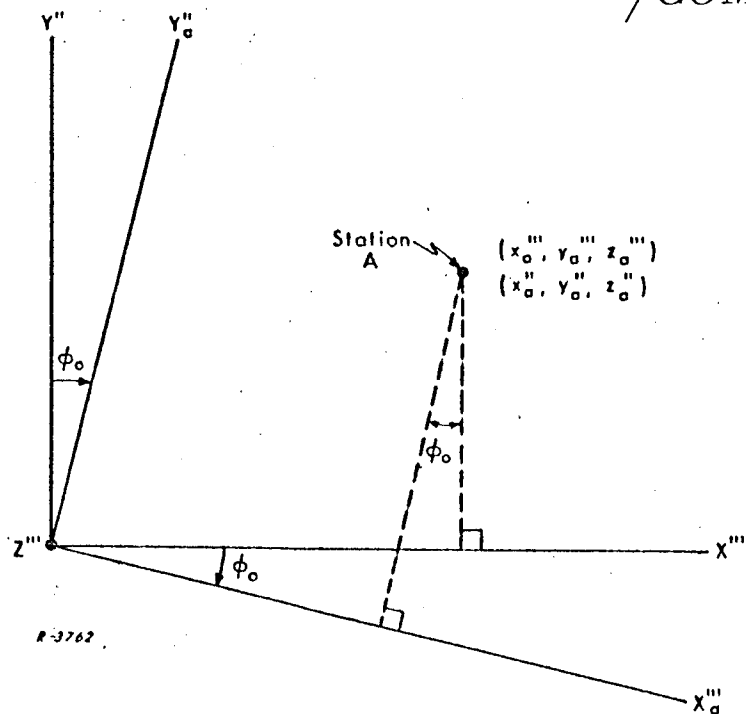


Fig. 19 Rotation of Coordinate System About Z''' Axis

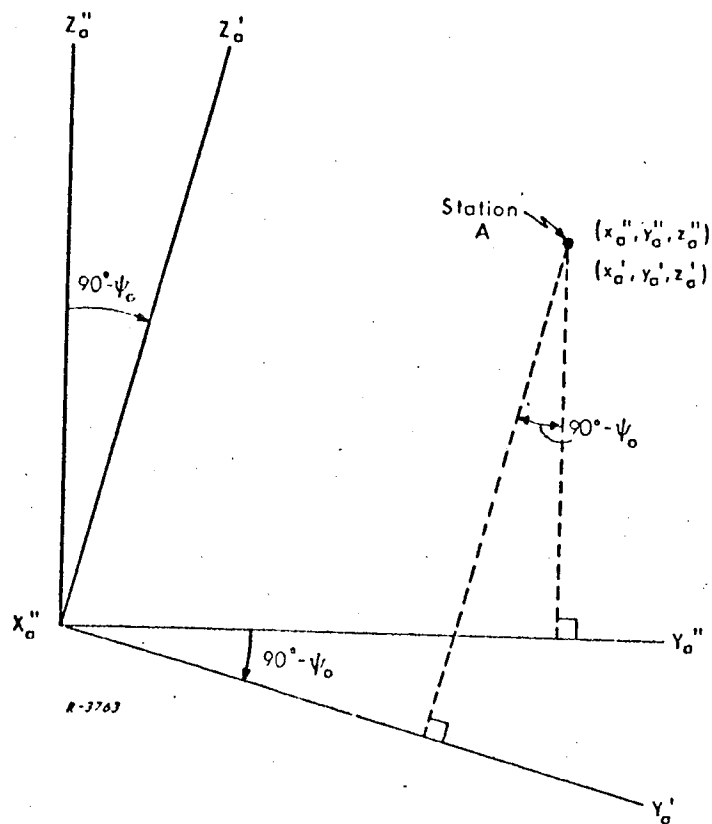


Fig. 20 Rotation of Coordinate System About X''_a Axis

translated from an earth-center reference to one near the surface of the earth, and the coordinate system described in Sec. 5.3 (see Fig. 16) is realized:

$$x_a = x'_a \quad (55)$$

$$y_a = y'_a \quad (56)$$

$$z_a = z'_a - R_o \quad (57)$$

Grouping terms in Eqs. (49) through (57)

$$x_a = x_a''' \cos \phi_o - y_a''' \sin \phi_o \quad (58)$$

$$y_a = (x_a''' \sin \phi_o + y_a''' \cos \phi_o) \sin \psi_o - z_a''' \cos \psi_o \quad (59)$$

$$z_a = (x_a''' \sin \phi_o + y_a''' \cos \phi_o) \cos \psi_o + z_a''' \sin \psi_o - R_o \quad (60)$$

By substitution of the appropriate ground station subscript in place of the subscript "a" in Eqs. (46) through (60), these equations become generalized coordinate translation formulas for any AROD ground station. As a convention, when the station location or coordinate system center is defined by west longitude, ϕ is positive; when east longitude, ϕ is negative. When the station location or coordinate system center is defined by north latitude, ψ is positive; south latitude defines ψ negative. Using these conventions, Eqs. (46) through (60) are valid for any worldwide location.

It should be reiterated that the actual station coordinate translation computation process, as developed in this section, is accomplished prior to vehicle launch. The coordinates defined by Eqs. (58), (59), and (60) are inserted in the vehicle-borne computer while it is on the ground, or may be loaded into the computer storage matrix while the vehicle is in flight utilizing a radio command link.

The data handling capability of the AROD tracking system up-link could feasibly accommodate the transmission of station coordinate data.

5.5 Vehicle Position Computation

Once the AROD ground station coordinates have been inserted in the vehicle computer, only the measurement of slant range from the vehicle to the ground stations is necessary for the computation of the vehicle position. A three-station solution is considered in this section.*

Referring to Fig. 16, the position of the vehicle with respect to the computer coordinate system center is defined by the vector \bar{S} . S_a , S_b , and S_c represent the slant range measurements to Stations A, B, and C, respectively. The linear quantities x , y , and z describe the vehicle position in the coordinate system of the vehicle computer. It is these quantities whose solution is sought. The quantities x , y , and z , each with subscripts a , b , and c , are the coordinates of Stations A, B, and C computed in Eqs. (58) through (60). Writing the system equations,

$$S_a^2 = (x - x_a)^2 + (y - y_a)^2 + (z - z_a)^2 \quad (61)$$

$$S_b^2 = (x - x_b)^2 + (y - y_b)^2 + (z - z_b)^2 \quad (62)$$

$$S_c^2 = (x - x_c)^2 + (y - y_c)^2 + (z - z_c)^2 \quad (63)$$

$$|\bar{S}|^2 \equiv S^2 = x^2 + y^2 + z^2 \quad (64)$$

* A four-station solution, determined by the weighted average of the components of three-station solution permutations, may actually be desirable and is recommended for future investigation. In addition to vehicle position computations, it is desirable to utilize the vehicle-borne computer to calculate a vehicle velocity vector using AROD system obtained range rate measurements from the three ground stations, and to translate the vehicle position measurements made in the cartesian coordinate system back to earth-center, polar coordinates. This computation, however, is beyond the scope of the discussion in Section 5.

The simultaneous solutions to this system of equations are of the form¹⁰

$$S^2 = \frac{-2\bar{P} \cdot \bar{Q} - 1}{2P^2} \pm \sqrt{(2\bar{P} \cdot \bar{Q} - 1)^2 - \frac{Q^2}{P^2}} \quad (65)$$

$$x = P_x S^2 + Q_x \quad (66)$$

$$y = P_y S^2 + Q_y \quad (67)$$

$$z = P_z S^2 + Q_z \quad (68)$$

where P_x , P_y , and P_z are constants for a station set, and Q_x , Q_y , and Q_z are factors containing constants and the measured quantities S_a , S_b , and S_c , and,

$$P^2 = P_x^2 + P_y^2 + P_z^2 \quad (69)$$

$$Q^2 = Q_x^2 + Q_y^2 + Q_z^2 \quad (70)$$

$$\bar{P} \cdot \bar{Q} = P_x Q_x + P_y Q_y + P_z Q_z \quad (71)$$

Now, we let

$$R_a^2 = x_a^2 + y_a^2 + z_a^2 \quad (72)$$

$$R_b^2 = x_b^2 + y_b^2 + z_b^2 \quad (73)$$

$$R_c^2 = x_c^2 + y_c^2 + z_c^2 \quad (74)$$

Substituting Eqs. (64), (72), (73), and (74) into Eqs. (61), (62), and (63), we obtain

$$\frac{S^2 + (R_a^2 - S_a^2)}{2} = x_a x + y_a y + z_a z \quad (75)$$

$$\frac{S^2 + (R_b^2 - S_b^2)}{2} = x_b x + y_b y + z_b z \quad (76)$$

$$\frac{S^2 + (R_c^2 - S_c^2)}{2} = x_c x + y_c y + z_c z \quad (77)$$

A simultaneous solution to Eqs. (75), (76), and (77) is of the form

$$x = \frac{x_{\text{num}}}{D} \quad (78)$$

$$y = \frac{y_{\text{num}}}{D} \quad (79)$$

$$z = \frac{z_{\text{num}}}{D} \quad (80)$$

From Eqs. (75), (76), and (77), the following determinant solutions to D , x_{num} , y_{num} , and z_{num} exist:

$$D = \begin{vmatrix} x_a & y_a & z_a \\ x_b & y_b & z_b \\ x_c & y_c & z_c \end{vmatrix} = x_a (y_b z_c - z_b y_c) + y_a (z_b x_c - z_c x_b) + z_a (y_c x_b - y_b x_c) \quad (81)$$

$$x_{\text{num}} = \begin{vmatrix} \mu_a & y_a & z_a \\ \mu_b & y_b & z_b \\ \mu_c & y_c & z_c \end{vmatrix} = \mu_a (y_b z_c - y_c z_b) + \mu_b (y_c z_a - y_a z_c) + \mu_c (y_a z_b - y_b z_a) \quad (82)$$

$$y_{\text{num}} = \begin{vmatrix} x_a & \mu_a & z_a \\ x_b & \mu_b & z_b \\ x_c & \mu_c & z_c \end{vmatrix} = \mu_a (x_c z_b - x_b z_c) + \mu_b (x_a z_c - x_c z_a) + \mu_c (x_b z_a - x_a z_b) \quad (83)$$

$$z_{\text{num}} = \begin{vmatrix} x_a & y_a & \mu_a \\ x_b & y_b & \mu_b \\ x_c & y_c & \mu_c \end{vmatrix} = \mu_a (x_b y_c - x_c y_b) + \mu_b (x_c y_a - x_a y_c) + \mu_c (x_a y_b - x_b y_a) \quad (84)$$

where:

$$\mu_a = \frac{S^2 + (R_a^2 - S_a^2)}{2} \quad (85)$$

$$\mu_b = \frac{S^2 + (R_b^2 - S_b^2)}{2} \quad (86)$$

$$\mu_c = \frac{S^2 + (R_c^2 - S_c^2)}{2} \quad (87)$$

Now, defining the following "P" constants,

$$P_{ax} = \frac{y_b z_c - y_c z_b}{D} \quad (88)$$

$$P_{bx} = \frac{y_c z_a - y_a z_c}{D} \quad (89)$$

$$P_{cx} = \frac{y_a z_b - y_b z_a}{D} \quad (90)$$

$$P_{ay} = \frac{x_c^z z_b - x_b^z z_c}{D} \quad (91)$$

$$P_{by} = \frac{x_a^z z_c - x_c^z z_a}{D} \quad (92)$$

$$P_{cy} = \frac{x_b^y y_a - x_a^y y_b}{D} \quad (93)$$

$$P_{az} = \frac{x_b^y y_c - x_c^y y_b}{D} \quad (94)$$

$$P_{bz} = \frac{x_c^y y_a - x_a^y y_c}{D} \quad (95)$$

$$P_{cz} = \frac{x_a^y y_b - x_b^y y_a}{D} \quad (96)$$

Combining Eqs. (78) through (96),

$$\begin{aligned} x = \mu_a P_{ax} + \mu_b P_{bx} + \mu_c P_{cx} &= \left(\frac{P_{ax} + P_{bx} + P_{cx}}{2} \right) S^2 + \frac{1}{2} \left[P_{ax} (R_a^2 - S_a^2) \right. \\ &\quad \left. + P_{bx} (R_b^2 - S_b^2) + P_{cx} (R_c^2 - S_c^2) \right] \end{aligned} \quad (97)$$

$$\begin{aligned} y = \mu_a P_{ay} + \mu_b P_{by} + \mu_c P_{cy} &= \left(\frac{P_{ay} + P_{by} + P_{cy}}{2} \right) S^2 + \frac{1}{2} \left[P_{ay} (R_a^2 - S_a^2) \right. \\ &\quad \left. + P_{by} (R_b^2 - S_b^2) + P_{cy} (R_c^2 - S_c^2) \right] \end{aligned} \quad (98)$$

$$z = \mu_a P_{az} + \mu_b P_{bz} + \mu_c P_{cz} = \left(\frac{P_{az} + P_{bz} + P_{cz}}{2} \right) S^2 + \frac{1}{2} \left[P_{az} (R_a^2 - S_a^2) + P_{bz} (R_b^2 - S_b^2) + P_{cz} (R_c^2 - S_c^2) \right] \quad (99)$$

It is seen that Eqs. (97), (98), and (99) conform to the general form of Eqs. (66), (67), and (68). Therefore,

$$P_x = \frac{P_{ax} + P_{bx} + P_{cx}}{2} \quad (100)$$

$$P_y = \frac{P_{ay} + P_{by} + P_{cy}}{2} \quad (101)$$

$$P_z = \frac{P_{az} + P_{bz} + P_{cz}}{2} \quad (102)$$

$$Q_x = P_{ax} R_{sa} + P_{bx} R_{sb} + P_{cx} R_{sc} \quad (103)$$

$$Q_y = P_{ay} R_{sa} + P_{by} R_{sb} + P_{cy} R_{sc} \quad (104)$$

$$Q_z = P_{az} R_{sa} + P_{bz} R_{sb} + P_{cz} R_{sc} \quad (105)$$

where

$$R_{sa} = \frac{R_a^2 - S_a^2}{2} \quad (106)$$

$$R_{sb} = \frac{R_b^2 - S_b^2}{2} \quad (107)$$

$$R_{sc} = \frac{R_c^2 - S_c^2}{2} \quad (108)$$

To compute the values of x , y , and z , it is necessary first to evaluate the denominator D as defined in Eq. (81). Next, the "P" constants defined in Eqs. (88) through (96) are evaluated. Eqs. (100) through (108) are then substituted into Eqs. (69), (70), and (71) to obtain the values of P^2 , Q^2 , and $\bar{P} \cdot \bar{Q}$. The value of S^2 is then obtained by substituting the computed values of P^2 , Q^2 , and $\bar{P} \cdot \bar{Q}$ into Eq. (65). Finally, the numerical values of x , y , and z are computed by substituting the computed values of P , S^2 , and Q into Eqs. (66), (67), and (68).

The computation process described above is physically carried out in the vehicle-borne computer while the vehicle is in flight. The calculated values of x , y , and z are converted back to an earth-center coordinate system, and the converted values may be telemetered to ground stations (feasibly utilizing the data transmission capability of the AROD system S-band down link) or coupled to the vehicle navigation system for in-flight vehicle navigation corrections.

5.6 Vehicle Position Errors Due to Inaccuracies in Station Coordinates

At least three error sources contribute potentially to the overall error in the computed vehicle position: (1) errors contributed by the vehicle-borne computer, (2) AROD system measurement errors (including both equipment and propagation errors), and (3) errors in ground station coordinates. Geometrical dilution will magnify those errors which exist in AROD slant range measurements and ground station coordinates.

It is reasonable to assume that with sufficiently sophisticated vehicle-borne computer hardware, no significant vehicle position error will be contributed by the computer itself. Measurement errors contributed by the AROD system, as well as those due to transmission of the tracking signals through the propagation medium, have been the subject of some limited analysis in the past. The effects of errors in AROD ground station coordinates, and of geometrical dilution in the position determination problem, however, have not been studied in detail. It is

not the intent of this section to analyze the effects of this latter potential error source; rather, the accuracy with which it is possible to locate ground stations with current geodetic techniques will be discussed briefly. The translation of probable ground station coordinate errors to the expected error in vehicle fixing, considering geometrical dilution, is a subject for recommended future investigation.

It will be recalled that the geocentric description of an AROD system ground station consists of geocentric longitude, geocentric latitude, and geocentric radius. Errors in these three parameters stem in general from three sources:⁹ (1) surveys from local control points, (2) surveys to datum origin, and (3) error in distance to earth's center.

5.6.1 Local Control Errors

The quality of the local tie of the ground station to its control network seldom introduces considerable error into its position with respect to other stations. Other sources of error are relatively much larger. Errors resulting from this source are generally less than one meter.

5.6.2 Errors to Datum Origin

Estimates of errors from this source are based primarily on an empirically derived mathematical technique known as Simmons' formula.¹¹ Simmons' formula has been employed, for example, for the conversion of Cape Kennedy Datum and Indian Datum to the European Datum, since no estimates of the uncertainty of the conversion constants are available. The estimates made by Simmons' rule should be conservative.

5.6.3 Errors to Earth's Center

The accuracy assessment, "To Earth's Center", is an RMS sum of the standard errors estimated for the tie to local control, to datum origin, and the following factors:

- (1) Uncertainty of the datum origin with reference to the earth's center. This uncertainty has been estimated as 50 meters for the major geodetic datums, 100 meters for the Australia Datum, and 120 meters for islands without geodetic ties to major datums. The uncertainty of the vertical datum is often difficult to assess. All stations have presumably been referenced to mean sea level. This may mean a net adjusted to many tide gauges with long periods of observation. Other datums based on good observations of mean sea level should differ by less than a meter.
- (2) Uncertainty of equatorial radius. This uncertainty has been estimated at between 25 and 100 meters, depending on the spheroid assumed.
- (3) Uncertainty of geoidal height. This uncertainty has been estimated at between 12 and 25 meters, depending on the source of information. Uncertainty in astro-geodetically determined geoidal heights varies between 12-18 meters.

5.6.4 Positional Accuracy of Ground Stations

The effect of the errors discussed in Secs. 5.6.1 through 5.6.3 is manifested in the estimated standard error in location between ground station pairs. This error is calculated as the root sum of squares of the individual errors contributing to the inaccuracy of the location of one station with respect to the other. It is reasonable to examine the accuracy of current geodetic surveys on an operational tracking station network in order to determine the probable magnitude of positional errors which could be expected for AROD ground stations. A summary of errors for stations in the NASA Manned Space Flight Network thus follows in succeeding paragraphs.⁹

Horizontal errors between Manned Space Flight Network stations on the North American Datum are estimated at between 8 and 38 meters, depending on the particular station pair. (The estimated standard error between Patrick AFB and Eglin AFB is 8 meters; between Bermuda and Pt. Arguello, 38 meters.) The

approximate error between stations on the North American Datum connecting to Kauai is on the order of 108 meters due to an estimated AMS occultation tie error of 100 meters.

Errors between stations on different datums are based on the root sum of squares of the individual errors to the Earth's center. Spherical standard errors between stations in the Manned Space Flight Network located on different datums are estimated at between 121 meters (Patrick AFB and Woomera) and 177 meters (Ascension Islands and Grand Canary).

5.6.5 Conclusions

It can be seen by the foregoing discussion that in many cases the theoretical accuracy of the AROD system (possibly even including propagation errors) is at least an order of magnitude better than that with which it is possible to locate ground stations, one with respect to the other. This observation suggests two interesting conclusions:

- (1) More accurate ground station surveys may be required in order to employ the full accuracy capabilities of the AROD system, and
- (2) It may be possible with the use of the AROD system to perform to the required accuracy these ground station surveys.

This latter possibility offers promise to the geodesist of a powerful new surveying instrument with which it may be possible to connect major datums with considerably more accuracy than present geodetic instrumentation permits.

5.7 Recommendations for Further Study

The preliminary investigation reported in Section 5 has brought about realization of the need for specific further study concerning the ultimate development of a vehicle-borne computer. Important steps in this development process are the following recommended studies, listed in the suggested chronological order of completion:

- (1) It is recommended that an exhaustive analysis of errors in the AROD system be conducted. As envisioned, this analysis would include all range and range-rate errors contributed by delivered AROD equipment, as well as signal propagation errors.
- (2) It is recommended that an analysis be conducted of the probable error in vehicle position due to AROD system errors (including both equipment and propagation errors), ground station location errors, and geometrical dilution.
- (3) It is recommended that the analysis conducted in Sec. 5.5 of this Technical Report be expanded to include the correction of vehicle position for movement of the vehicle during the signal transit time.
- (4) It is recommended that a methodology be developed for obtaining the four-station vehicle solution suggested in the footnote to Sec. 5.5 of this Technical Report.
- (5) It is recommended that an appropriate analysis be conducted to develop the methodology for in-flight computation of the vehicle velocity vector.
- (6) It is recommended that a coordinate system be developed for in-flight translation of the vehicle position in cartesian coordinates to earth-center form.
- (7) Finally, it is recommended that a study be conducted to determine the optimum system design of a special-purpose, vehicle-borne computer whose function is to compute the vehicle velocity vector and vehicle position corrected for vehicle movement during the signal transit time, then translate this information in cartesian form to earth-center polar form.

REFERENCES

1. Motorola, Inc., Military Electronics Division, "AROD System Description," Report No. 3065-2-1, Prepared for MSFC, Contract No. NAS8-11835, Revisions 1, 2, 3, 4 from 4 June 1965 to 1 March 1966.
2. Kline, A. J., "AROD Vehicle Tracking Receiver Design," Technical Memorandum No. 3065-26, 3 August 1966, Government Electronics Division, Aerospace Center, Motorola, Inc.
3. ADCOM, Inc., "Special Studies of AROD Systems, Concepts and Designs," TR No. 1, NASA Contract No. NAS8-20128, January 1967.
4. ADCOM, Inc., Monthly Progress Letter Report No. 18, Contract No. NAS8-20128, NASA Marshall Space Flight Center, December 19, 1966.
5. Philco Research Division, Document RADC-TN-60-280, Rome Air Development Command, U.S. A. F.
6. J. J. Freeman Associates, Inc., NAS5-1404, NASA Goddard Space Flight Center, 1963.
7. National Defense Research Council, Summary Technical Report of the Committee on Propagation, Vol. 1 (Chapter 13), Washington, D. C., 1946.
8. Lawrence, R. S., Little, C. G., Chivers, H. J. A., "A Survey of Ionospheric Effects Upon Earth-Space Radio Propagation," Proc. IEEE, pp. 4-27, January 1964.
9. Goddard Directory of Tracking Station Locations, NASA Document No. X-554-64-176 (MSFC No. NASA TM X-55124), Goddard Space Flight Center, Greenbelt, Maryland, 1 July 1964.
10. Saunders, Grady H., "AROD Tracking and Navigation System," Research Achievements Review Series No. 17, NASA TM-53540, George C. Marshall Space Flight Center, Huntsville, Alabama, pp. 9-24, 1966.
11. Simmons, Lansing G., "How Accurate is First Order Triangulation," The Journal Coast and Geodetic Survey No. 3, April 1950.